catalysts

MDPI

*Review*

# Biocatalysis as a Green Approach for Synthesis of Iron Nanoparticles—Batch and Microflow Process Comparison

**Maja Benković *, Davor Valinger, Tamara Jurina, Jasenka Gajdoš Kljusurić and Ana Jurinjak Tušek**

Faculty of Food Technology and Biotechnology, University of Zagreb, Pierottijeva 6, 10000 Zagreb, Croatia
* Correspondence: maja.benkovic@pbf.unizg.hr

**Abstract:** There is a growing need for production of iron particles due to their possible use in numerous systems (e.g., electrical, magnetic, catalytic, biological and others). Although severe reaction conditions and heavy solvents are frequently used in production of nanoparticles, green synthesis has arisen as an eco-friendly method that uses biological catalysts. Various precursors are combined with biological material (such as enzymes, herbal extracts, biomass, bacteria or yeasts) that contain chemicals from the main or secondary metabolism that can function as catalysts for production of nanoparticles. In this work, batch ("one-pot") biosynthesis of iron nanoparticles is reviewed, as well as the possibilities of using microfluidic systems for continuous biosynthesis of iron nanoparticles, which could overcome the limitations of batch synthesis.

**Keywords:** iron nanoparticle; green synthesis; batch ("one-pot") biosynthesis; continuous microfluidic nanoparticle synthesis



**Citation:** Benković, M.; Valinger, D.; Jurina, T.; Gajdoš Kljusurić, J.; Jurinjak Tušek, A. Biocatalysis as a Green Approach for Synthesis of Iron Nanoparticles—Batch and Microflow Process Comparison. *Catalysts* **2023**, *13*, 112. https://doi.org/10.3390/catal13010112

Academic Editor: Anwar Sunna

Received: 29 November 2022
Revised: 21 December 2022
Accepted: 2 January 2023
Published: 4 January 2023



## 1. Introduction—The Definition of Nanotechnology

Nanotechnology includes the science, technology, production, processing, design and analysis of materials with sizes from 1 to 100 nanometers. Nanomaterials include nanoparticles, nanotubes, fullerenes and different types of nanofibers. Nanoparticles contain components whose three dimensions must be 100 nm or less [1,2]. Nanomaterials are defined as insoluble, biologically stable materials with one or more external dimensions or an internal structure ranging in size from 1 to 100 nm.

Nowadays, many nanoparticles are successfully synthesized on an industrial level: silver, palladium, iron, titanium, carbon, manganese oxide, copper, etc. [3–5]. The biggest issue concerning synthesis of those particles is use of many solvents and chemicals that are often harmful to the environment. Because of that, in recent years, scientists are exploring "green" ways of nanoparticle synthesis, one of them being biocatalysis using herbal extracts, yeasts, fungi and bacteria. The aforementioned organisms produce secondary metabolites (bioactives) capable of acting as biocatalysts and capping agents for synthesis of nanoparticles. Among others, silver, calcium, iron, copper, zinc and gold nanoparticles can be synthesized using the green biocatalysis approach [6–12]. Among them, iron nanoparticles have a wide array of application in agriculture (nanoadditives, nanofertilizers, nanosensors, nanopesticides and herbicides) [13]; food industry (analysis of food, enzyme immobilization, protein separation and purification) [14]; and pharmaceutical industry and biomedicine (drug delivery, anticancer, antiviral and antimicrobial agent development) [15]. Furthermore, their biosynthesis is considered to be simple, with no aggressive chemicals needed, feasible and resulting in iron nanoparticles whose properties can be regulated using different process conditions, such as pH, temperature, time or precursors [16]. This review paper is focused on biocatalytic synthesis of iron nanoparticles using two approaches: batch synthesis and continuous micro-flow synthesis. Throughout the review, as an introduction, basic aspects of the synthesis process of nanoparticles in general will be addressed, followed by a description of the biosynthesis specific for iron

nanoparticles as well as a description of "green" biocatalytic synthesis in batch ("one-pot") conditions and green biosynthesis in continuous microsystems.

## 2. General Approaches to Nanomaterial Production

Production of nanomaterials can be divided into two categories: "top down" and "bottom up" [2]. "Top down" production of nanomaterials involves crushing particles of larger dimensions to nano sizes using various physical and chemical methods [17]. "Top down" processes include sputtering, laser ablation, etching, electro-explosion or mechanical grinding [16]. An example of this type of production is mechanical grinding, which is used to shred wheat bran as a potential bioactive food ingredient, which results in enhancement of their bioactive action [18]. Dry grinding to nano size is also used in grinding of green coffee, which enhances its antioxidant activity [19]. Homogenization is also described as one of the most effective "top down" methods, and it is applied mostly in the dairy industry. Pairing a laser in combination with cooling as a "top down" method is also mentioned in the literature [20]. Plus sides of the top down processes include the ability to produce particles with low contamination and well-defined shapes and sizes, as well as the possibility to control the stability, shape and size of nanoparticles by controlling the process conditions (e.g., pH, temperature, time, etc.) [21]. Downsides include costly equipment, which makes the process economically unsustainable, and use of solvents, which makes the process environmentally unfriendly [16,22,23].

The "bottom up" approach is applied as an alternative to the "top down" process, where synthesis begins at an atomic level through self-assembly of atoms into new nuclei, and growth of nanoparticles continues to a desired size or shape [21]. Some of the processes included are aerosol-based processes, laser pyrolysis, sol–gel process, spinning, green synthesis, atomic and molecular condensation, supercritical fluid synthesis, co-precipitation, mineralization, flow injection, sonochemical synthesis, microemulsions, etc. [10,16]. This approach can result in complex molecular structures that arise as a result of self-organization. Casein micelles are an example of independent organization and structuring of biological compounds resulting in stable nanomaterials [24]. Downsides of the "bottom up" approaches include formation of nanoparticles whose shape and size cannot be completely controlled since most of them are synthesized based on self-arrangement of the particles at the molecular level. Furthermore, after synthesis, nanoparticles need to be purified and isolated from the reaction mixture, which is often hard and with very low recovery [16,25]. Moreover, some of these processes include use of organic solvents, which are considered to be damaging to the environment and have to be performed at harsh reaction conditions (high temperature, high pressure, high acidity, etc.). However, green synthesis or biocatalysis is one of the "bottom up" processes with a promising future perspective since it excludes use of heavy solvents and enables use of biological materials for nanoparticle synthesis and is often described as safe, cost-effective and easy to perform [10,22,26].

## 3. Iron Nanoparticles

Iron nanoparticles are non-toxic particles with excellent dimensional stability, high catalytic activity, high magnetism, high thermal and electrical conductivity, high surface area and high microwave adsorption ability [16,27]. However, iron nanoparticles are prone to oxidation, which is described as their greatest weakness [28]. The classification of iron nanoparticles is shown in Figure 1.

Iron nanoparticles have multiple possible applications, which are largely dependent on the type of iron nanoparticle. Some examples of their application include: (i) magnetic and electrical applications (transformers, inductors, magnetic recording heads, electromagnets, motors and other electrical components); (ii) application in catalytic reactions (hydroformylation of an alkene, hydrogenation of naphthalene, conversion of nitrogen compounds to $N_2$ during coal pyrolysis, degradation of trichloroethylene, growth of gallium nitride nanostructures and growth of carbon nanotubes); (iii) biomedical applications (magnetic resonance imaging, biological staining, drug delivery, pollutant adsorption, gene therapy,

antimicrobial agent, etc.) [16,28]; food applications (food preservation and analysis, enzyme immobilization, protein separation and purification) [14] and agriculture applications (nanoadditives, nanofertilizers, nanosensors, nanopesticides and herbicides) [13]. Because of their wide range of applications, there is an emerging need for synthesis of iron particles. As mentioned earlier, synthesis of nanoparticles often includes heavy solvents and harsh reaction conditions, but green synthesis has emerged as an environmentally friendly type of synthesis using biological material as catalysts. This type of synthesis will be discussed further in this review paper.

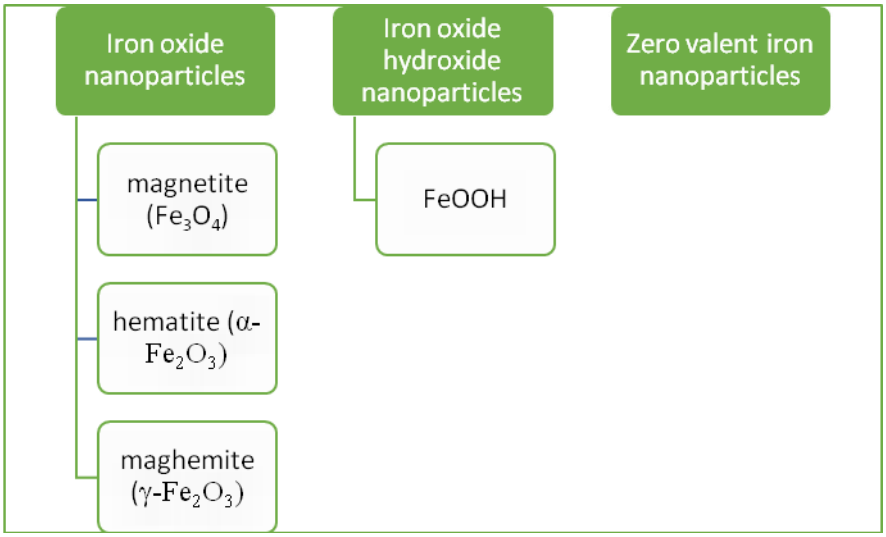


**Figure 1.** Classification of iron nanoparticles.

## 4. Green Synthesis of Iron Nanoparticles

Green synthesis includes different precursors that are mixed with biological material (e.g., enzymes, herbal extracts, biomass, bacteria or yeasts) that contains molecules from their primary or secondary metabolism. These molecules can act as catalysts for formation of nanoparticles. According to literature data, bacteria, fungi, algae and plants mixed with a precursor solution can be used for green synthesis of nanoparticles [7,29]. Synthesis can occur via extracellular and intracellular mechanisms [10].

Bacteria-mediated synthesis of iron nanoparticles is described in a review paper (Ash and coworkers [30]) as a result of two possible pathways: biologically induced biomineralization (extracellular), where magnetite crystals are formed in the culture solution as a by-product, and biologically controlled biomineralization (intracellular). Extracellular processes can be mediated using Fe(III)-reducing bacteria (*Geobacter metallireducens*, *Shewanella putrifaciens*, *Thermoanaerobacter ethanolicus*, *Archaeoglobus fulgidus*, *Desulfuromonas acetoxidans*) and sulfate reducing bacteria (*Desulfuromonas*, *Actinobacter*), where bacterial metabolites exerted from the cell act as reducing agents. The intracellular processes occur within the cytoplasm or the cell wall. The specific ions must be transferred inside the cell where nucleation occurs, and the crystal formation is under strict control of the micro-organism [30]. Furthermore, Nadeem and coworkers [31] mention synthesis of iron nanoparticles using *Bacillus cereus*, *Staphylococcus warneri*, *Bacillus subtilis* and *Lactobacillus casei* for extracellular synthesis [31–33] and *Lactobacillus fermentum* and *Gluconacetobacter xylinus* for intracellular synthesis [31,34,35].

Fungi-mediated synthesis or mycosynthesis occurs when fungi secrete bioactive compounds that act as biocatalysts for formation of nanoparticles. Furthermore, fungi are considered as excellent nanosynthesis mediators because of their high growth rate [29]. Although the mechanisms of nanoparticle formation using fungi are not yet fully understood [36], it is considered that, similar to bacteria, synthesis can occur extracellularly and intracellularly [31]. Usually, cells are first grown, filtered and washed, after which the cells are removed by filtration and cell-free extract is mixed with precursors to synthesize

nanoparticles [37]. Among others, *Trichoderma asperellum*, *Phialemoniopsis ocularis*, *Fusarium incarnatum*, *Aspergillus flavus Aspergillus niger*, *Rhizopus stolonifera*, *Penicillium oxalicum*, *Alternaria alternata* and *Candida bombicola* have been reported to be successfully used for synthesis [29,37–41]. According to Adeleye et al. [42] and Nadeem et al. [31], functional groups such as thiol, carboxylic acid, hydroxyl and alkyl groups were responsible for synthesis and stabilization of the nanoparticles.

Algae are eukaryotic photoautotrophic organisms harvested from seas. Since they are capable of producing secondary bioactive metabolites, which can act as reducing, capping and stabilizing agents, they can be used in production of NPs. Furthermore, because of their rapid grow rate, red, green and brown algae are often considered to be the best choice for NP synthesis [43]. The synthesis procedure can be described by three main steps: (i) production of the algal extract, (ii) preparation of precursor solutions of ionic metallic compounds and (iii) mixing and incubation of algal extracts and precursor solution at defined experimental conditions (pH, temperature, duration and mixing) [44,45]. Win et al. [46] reported synthesis of $Fe_3O_4$ nanoparticles using *Chlorella*-K01 extract with a yield of 16–829 mg of $Fe_3O_4$ NP depending on the pH of the reaction mixture (pH = 6–12). El Kassas et al. [47] used extracts of seaweeds *Padina pavonica* (Linnaeus) Thivy and *Sargassum acinarium* (Linnaeus) Setchell 1933 for synthesis of iron oxide NPs from $FeCl_3 \cdot 6H_2O$ precursors, while Salem et al. [48] reported synthesis of spherically shaped $Fe_3O_4$ NP with a size of 22.22–33.33 nm using the algae *Jania rubens*. Aside from synthesis of iron NP, there have been numerous reports of synthesis of Ag, Au, Cu and Zn NPs using algal extracts such as *Bifurcaria bifurcate*, *Galaxaura elongate*, *Sargassum plagiopyhllum*, *Caulerpa racemose*, *Ulva fasciata*, etc. [44,49].

Abundance of plants and their bioactive properties make them a very desirable and cheap source of biocatlysers for NP synthesis [50]. Plant parts that can be used include root, stems, leaves, flower, seed, wood, the whole plant or any other part of the plant that contains bioactives that can reduce the iron precursor [10,16,50]. Bioactive molecules derived from plants that have the ability to reduce metal precursor solutions include phenols, tannins, saponins, alkaloids, organic acids, flavonoids, sugars, proteins, vitamins, terpenoids and free amino acids [10,16,22,26]. Synthesis of Fe NPs is referred to as "one-pot" synthesis [22], which occurs extracellularly, and the most common procedure involves several steps: (i) preparation of the herbal extract, (ii) synthesis of nanoparticles by mixing extracts with iron precursor solutions at desired conditions and (iii) separation and purification of the nanoparticles. The proposed mechanism of formation of the NPs is bondage of iron ions to bioactive compounds, which then reduce iron atoms, and formation of the iron nucleus occurs [16]. It is important to mention that the catalytic reaction using plant extracts is faster in comparison to the microbe reaction; the time required for synthesis ranges from a few minutes to a few hours and depends on plant type and concentration of bioactives in a given plant [25]. *Prunus persica*, *Agrewia optica*, *Citrus macroptera*, *Cynometra ramiflora*, *Eucalyptus globules*, *Lawsonia inermis* (Henna), *Syzygium cumini*, saffron plant, apple, apricot, avocado, cherry, kiwi, lemon, pine, pomegranate, oak, olive, black tea, green tea, vine, peach, pear, *Hibiscus rosa sinensis*, *Artocarpus heterophyllus*, *Lagenaria siceraria* and *Moringa oleifera* are only some of the numerous examples of plants that can be used to synthesize Fe NPs [22,23,26,51–61].

## 5. Batch ("One-Pot") Biosynthesis of Iron Nanoparticles

### *5.1. Batch Synthesis Using Herbal Extracts*

Batch synthesis is considered to be the most efficient and environmentally friendly procedure for synthesis of iron nanoparticles. Since the whole synthesis is actually performed in one beaker, glass, pot or reactor, it is often referred to as "one-pot" synthesis. A schematic diagram of the process is shown in Figure 2. Moreover, in comparison to synthesis using bacteria and fungi, it is considered to be much simpler since the step where bacterial and fungal biomass has to be synthesized and maintained under aseptic conditions [62] is not present, and preparation of herbal extracts is much simpler.

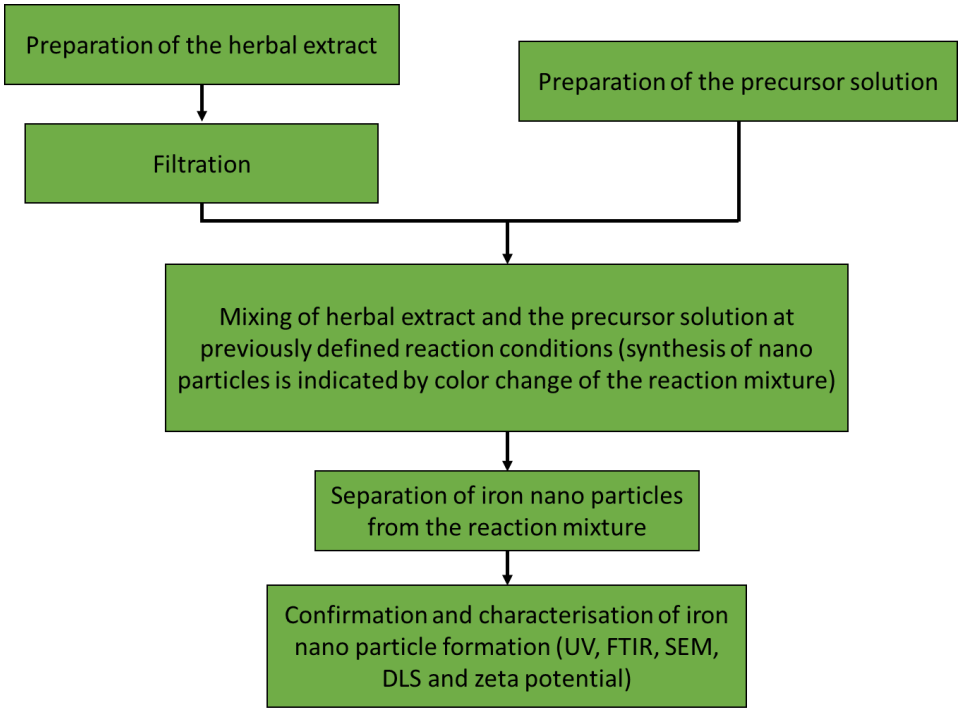


**Figure 2.** Flow diagram of batch synthesis of iron nanoparticles using herbal extracts.

Green synthesis of iron nanoparticles using plants and algae starts with preparation of the extracts and the precursor solutions (Figure 2). According to literature data, compounds such as mimosine, mimosinic acid, tyrosine, carotenoids, terpenoids, flavonoids, tannins, alkaloids, glycosides, vitamins, quercetin, phytosterol, rutin, apigenin, chlorogenic acid, gallic acid, vanillic acid, cinnamic acid, catechol, ferulic acid, theanine, theobromine, caffeine, anthocyanins, gallocatechins, proanthocyanidin, ellagic acid, chebulagic acid, eugenol, nerol, kaempferol and many more have been identified as compounds with functional groups that can act as reductant and capping/stabilizing agents for iron nanosynthesis [9].

The mechanism of action of the bioactive compounds has not yet been completely explored, but studies show that natural antioxidants reduce iron ions to iron nanoparticles and can bind to the surface of the nanoparticles as stabilizing and capping agents, improving their physicochemical properties [63–65]. As precursor solutions, $FeCl_3 \cdot 6H_2O$, $FeCl_2 \cdot 4H_2O$, $FeSO_4 \cdot 7H_2O$, and $Fe(NO_3)_3 \cdot 9H_2O$ can be used in different concentrations (0.01 M–0.1 M) [10,16,22,23]. After the solutions have been prepared, the extract is filtered and mixed with the precursor solution to begin synthesis. It is important to note that the yield of the iron particles is highly dependent on the process conditions (pH, temperature, extract concentration, extract antioxidant capacity, precursor solution concentration, extract: precursor ratio, time, etc.), and the process has to be optimized. The effect of pH has been addressed in several studies, with contradictory results. For example, Ebrahiminezad and co-workers mention the effect of pH on particle size distribution and stability of INPs, saying that lower pH value enables production of iron NPs with smaller particle size and higher stability in comparison to the iron NPs produced at higher pH [16]. On the other hand, Lenders and co-workers reported the pH range 7–9 as optimal for INP synthesis using *Aeromonas hydrophila* [66], while Woznica and co-workers reported that extreme acidic and basic conditions retard synthesis of INPs [67]. A study by Huang et al. revealed that size and shape of particles can be controlled by regulating the pH of the reaction solution; the optimal synthesis conditions using green tea extract were defined as pH = 6.0 and T = 318 K [68]. Furthermore, Ebrahiminezhad et al. state that the presence of organic acids (oxalic and citric) increases the stability of iron nanoparticles [16]. Extract properties and the ratio of extract:precursor also affect formation of nanoparticles and the particle size distribution of the formed particles, as stated in various studies [16,64,69–73]. In general,

higher concentration of bioactive compounds that are available to reduce Fe in the extract also means higher rate of synthesis. However, too high extract:precursor ratio and too high extract concentration lead to INP instability in terms of agglomeration of iron NPs to larger clusters of particles as excess reducing agents can cause secondary reduction on the surface of formed nuclei and thus the need for process optimization [6,10,16,26,72]. Patra and co-workers investigated the effect of temperature on synthesis of iron nanoparticles and concluded that synthesis is much faster at higher temperatures [74]. However, one needs to be careful with temperature increase since many bioactive compounds used as reducing and capping agents tend to be heat-sensitive; e.g., Rajendran and Sen reported that an increase in temperature beyond 40 °C resulted in poor synthesis rates, which they attributed to inactivation of bioactives [75]. It is important to emphasize that temperature sensitivity also depends on the type of extract used and the bioactives present in those extracts; e.g., Bibi et al. managed to synthesize INPs using *Punica granatum* seed extract at temperatures as high as 70 °C [76], and Khan and co-workers managed to synthesize INPs using *Mentha spicata* leaf extract at 100 °C [77]. Generally speaking, INPs can be synthesized at temperatures ranging from 25 to 100 °C, but, due to volatility of some bioactive catalysts, room temperature is considered to be the preferred temperature for synthesis [74]. Furthermore, the influence of temperature is also important during extract preparation since it affects the concentration of bioactives present in the extract. Higher extraction temperatures usually yield higher extraction efficiencies, but some studies emphasize that too high extraction temperature (>70 °C) leads to lower antioxidant capacity and, therefore, lower concentration of bioactive molecules, which can act as biocatalysts and capping agents [16]. Incubation time has also been reported to influence INPs particle size distribution and morphology: longer incubation times tend to lead to undesirable aggregation of the particles [10]. Salt used for preparation of the precursor solution as well as the concentration of the precursor solution both influence formation of INPs; type of Fe salt usually affects the time needed for INP synthesis, as well as INPs shape and size, while a decrease in the concentration of the precursor solution results in smaller particles [10,75,78,79].

Color change of the reaction mixture is usually an indicator that the nanoparticles have been synthesized. However, color change cannot be considered as the only confirmation that nanoparticles are present, and different analysis methods are used to identify the particles present in the mixture. One of the most widely used methods is continuous UV spectra of the reaction mixture. Fourier transform infrared spectroscopy (FTIR) is also used for confirmation of nanoparticle formation, with the basic aim to identify the exact chemical composition of the particles, while scanning electron microscopy (SEM) and transmission electron microscopy (TEM) are used to obtain insight into the structure of the particles and energy-dispersive X-ray spectra for crystallinity assessment. Furthermore, nanoparticle size can be determined using dynamic light scattering (DLS) as well as electron microscopy [10,22,26]. After the nanoparticles have been successfully characterized, they need to be separated from the reaction mixture, purified and dried, which is usually completed by sedimentation, centrifugation, filtration, washing of the particles using organic solvents and then drying in convective dryers or desiccators.

An overview of some studies performed in the last several years (2018–2022) involving green biosynthesis of INPs using plant extracts is shown in Table 1.

Based on the data shown in Table 1, there are many plant species that possess bioactive compounds that can be used as reducing and capping agents in synthesis of iron nanoparticles. However, since each plant is different, different reaction conditions are required for synthesis, and nanoparticles with different properties, morphologies and sizes can be produced. Since each plant is a story of its own, future research should be aimed toward screening of plants that can be used as precursors, as well as finding plants that can result in nanoparticles with the most controllable properties. Furthermore, most of the studies listed in Table 1 do not have a single well-defined compound that was identified as the capping agent; in most cases, only a general group of compounds is listed (e.g., phenolic

compounds, bioactives with antioxidant capacity, etc.). Therefore, one more aim of future research should be definition of an exact compound that has the highest capping potential so that the green synthesis processes can generate even higher yield.

**Table 1.** An overview of recent studies on iron nanoparticle synthesis using plant extracts.

| Plant | Precursor | Synthesis Conditions | Iron Nanoparticle Properties | Reference |
|---|---|---|---|---|
| *Ageratum conyzoides* (whole plant extract) | $FeCl_3 \cdot 6H_2O$ (0.1 M) solution | Room temperature, extract:precursor ratio: 1:1, t = 3 min | Cubic crystals, average diameter 85.98 nm | [80] |
| *Bauhinia tomentosa* (leave extract) | $FeCl_3$ (0.01 M) solution | Room temperature, extract:precursor ratio: 1:1, continuous stirring until visible color change | Crystalline particles, average diameter 70 nm | [81] |
| *Carica papaya* (leaves extract) | $FeCl_3 \cdot 6H_2O$ (0.1 M) solution | Room temperature, extract:precursor ratio: 1:1, t = 30 min, continuous stirring | Irregular, non-uniform crystalline particles, visible formation of agglomerates, average diameter 21.59 nm | [82] |
| *Platanus orientalis* (leaves extract) | $Fe(NO_3)_3 \cdot 9H_2O$ salt (99.8 %) | 1 g of $Fe(NO_3)_3 \cdot 9H_2O$ salt added to 10 mL leaf extract, t = 1 h, T = 25 °C, continuous stirring | Spherical shape with an average diameter of 38 nm | [83] |
| *Hibiscus rosa sinensis* (flowers extract) | $FeCl_2 \cdot 4H_2O$ (1 mM) solution | Precursor:extract ratio: 1:1, 1:2 and 1:3, t = 20 s microwave radiation | Crystalline nanoparticles of nearly spherical shape, polydisperse, average diameter 51 nm | [84] |
| *Artocarpus heterophyllus* (peel extract) | 0.1 M $FeCl_2$ solution | Precursor:extract ratio 2:3, room temperature, pH = 6 | Spherical particles, irregular surface, agglomerated, average diameter 33 nm | [85] |
| *Punica granatum* (seeds extract) | $FeCl_3$ (1 M) solution | Extract:precursor ratio 12:1, 70 °C for 15 min, continuous stirring | Aggregates, maximum distribution in the range of 28.4–66.2 nm | [76] |
| *Crocus sativus* (whole plant extract) | $FeCl_3$ (1 M) solution | Extract:precursor ratio 1:1, 60 °C for 30 min, continuous stirring | Nanoparticle structures with average grain sizes of 24.27–46.27 nm | [51] |
| *Quercus virginiana*, *Eucalyptus globulus* (leaves extract) | $FeCl_3$ solution (0.1 M) | Extract:precursor in a 2:1 ratio, room temperature, continuous stirring at 300 rpm | Spherical, particle diameter around 10–100 nm, amorphous structure | [86] |
| *Thymus vulgaris* L. (leaves extract) | $FeCl_3 \cdot 6H_2O$ (0.1 M) | extract:precursor ratio: 1:1, 5 min, room temperature | Spherical particles, bimodal distribution with peaks at 2 nm and 40 nm | [71] |
| *Vitex leucoxylon* (leaves extract) | $FeSO_4$ solution (0.05 mM) | extract:precursor ratio: 1:10, room temperature, incubated in the dark until a visible color change occurred | Spherical, with a diameter ranging from 45 nm to 100 nm based on SEM images | [87] |
| *Lawsonia inermis* (parts of the plant not identified, extract) | $FeSO_4 \cdot 7H_2O$ (0.02 M) solution | extract:precursor ratio: 1:1, 60 °C, pH = 11, 30 min | Spherical, average size 150–200 nm | [26] |
| *Syzygium cumini* (leaves extract) | $FeCl_3$ solution (0.01 M) | Precursor: extract ratios 1:1, 4:1 and 9:1, continuous stirring, room temperature | Spherical, average size 55–65 nm (SEM) | [22] |
| *Pittosporum undulatum*, *Melia azedarach*, *Schinus molle and Syzygium paniculatum (var. australe)* (leaves extract) | 0.1 M $FeCl_3 \cdot 6H_2O$ solution | 0.1 M $FeCl_3 \cdot 6H_2O$ solution was slowly introduced using a peristaltic pump with a flow rate of 2 mL/min, ensuring a 2:1 extract:precursor ratio, continuous mixing, room temperature | Irregular particles, chain-like structures, size dependant on the extract used (min. 5–10 nm formed using *Pittosporum undulatum* extract, max. >100 nm for *Schinus mole*) | [88] |
| *Apium graveolens* (stalks extract) and *Camellia sinensis* (leaves extract) | $Fe(NO_3)_2 \cdot 6H_2O$, 0.02 M solution | 75 °C initial temperature, reduced to 60 °C and incubated for 60 min | Irregular, cubic and hexagonal shapes of various sizes, visible aggregates, smooth surface, diameter raged from 30.52 to 95.14 nm | [89] |
| *Ficus carica* (leaves extract) | 0.01M $FeCl_3 \cdot 6H_2O$ solution | 40 mL of the extract added to 100 mL of the precursor solution, pH = 11, continuous stirring at 70 °C for 1h | Crystalline multiform particles, aggregates visible, diameter 43–57 nm | [90] |
| *Pometia pinnata* (leaves extract) | $FeCl_3 \cdot 6H_2O$ (0.01 M) solution | Extract:precursor ratio 1:1, 500 rpm, 25 °C, 2h, with (pH = 11) and without pH adjustment | Polydisperse amorphous magnetic particles, size 10–20 nm | [91] |
| *Camellia sinensis* (leaves extract) | $FeCl_3$ 0.01M solution | Extract:precursor ratio 1:1, room temperature | Particles of maximum diameter of 116 nm | [56] |
| *Garcinia mangostana* (fruit peel extract) | $FeCl_3 \cdot 6H_2O$, 97% and $FeCl_2 \cdot 4H_2O$ (0.99 g) at a molar ratio of 2:1 | pH = 11, 30 min, continuous stirring, different extract concentrations (1, 2, 5 and 10 % *w*/*w*) | Irregularly shaped magnetic particles, mean size of 13.42 ± 1.58 nm | [92] |

**Table 1.** *Cont.*

| Plant | Precursor | Synthesis Conditions | Iron Nanoparticle Properties | Reference |
|---|---|---|---|---|
| *Ocimum tenuiflorum* (leaves extract) | $FeCl_2 \cdot 4H_2O$ (1 mol) $FeCl_3 \cdot 6H_2O$ (2 mol) in 100 mL distilled water (solution) | 100 mL of precursor solution with 5 mL of extract heated at 80 °C with continuous stirring until color change | Nanospheres (3–5 nm), aggregates, and nanoelipsoidal particles with a diameter of 100–200 nm | [93] |
| *Sidacordifolia* (whole plant extract) | 0.07 M $Fe(NO_3)_2$ solution | 5 mL of the extract was added to 10 mL of the precursor solution, heated at 60 °C for 5 min under continuous stirring | Spherical nano clusters, hematite of average diameter 16 nm | [94] |
| *Azadirachta indica* (leaves extract) | $FeCl_3 \cdot 6H_2O$, $FeSO_4 \cdot 7H_2O$ (aqueous mixture of ferric ($Fe^{3+}$) and ferrous ions ($Fe^{2+}$) at a 2:1 molar ratio) | pH 10–11, 80 °C for 1 h with constant stirring | Spherical, uniform and particles smaller than 100 nm, aggregates visible | [95] |
| *Mentha spicata* (leaves extract) | $FeCl_3$, 0.4 M solution | Extract:precursor ratio 1:1, 100 °C, 30 min | Circular and rod-shaped nanoparticles with an average diameter 21–82 nm | [77] |
| *Citrus macroptera* juice extract | $FeCl_3$ 0.14 M solution | Not specified | Spherical particles with diameter of 12 nm | [61] |

### *5.2. Batch Synthesis Using Algae and Seaweed*

Similar to plants, algae also produce bioactive compounds capable of acting as reducing and capping agents for synthesis of iron nanoparticles, with the procedure of synthesis being very similar to the procedure described for plants (Figure 1). As mentioned earlier, the synthesis procedure can be described by three main steps: (i) production of the algal extract, (ii) preparation of precursor solutions of ionic metallic compounds and (iii) mixing and incubation of algal extracts and precursor solution at defined experimental conditions (pH, temperature, duration and mixing) [44,45]. Some examples of using algae for synthesis of nanoparticles are shown in Table 2.

**Table 2.** Some examples of use of algae for synthesis of iron nanoparticles.

| Algae | Precursor | Synthesis Conditions | Iron Nanoparticle Properties | Reference |
|---|---|---|---|---|
| *Ulva lactuca extract* | 0.1 M $FeCl_3$ solution | Extract:precursor ratio 1:1; 30 °C, 2 h, continuous stirring | Uniform, spherical, diameter 20–40 nm | [96] |
| *Colpomenia sinuosa* and *Pterocladia capillacea* extracts | 0.1 M $FeCl_3$ solution | Extract:precursor ratio 1:1; 800 rpm, room temperature for 1h (*C. sinuosa)* and 2 h (*P. capillacea)* | Nanospheres, diameter 16.85–22.47 nm | [97] |
| *Chlorella*-K01 extract | 0.1 M $FeCl_2 \cdot 4H_2O$ solution | Precursor:algal extract ratio 2:3, 6–70 °C, different pH values (6, 8, 10 and 12) | Spherical $Fe_3O_4$ nanoparticles, diameter in the range of approximately 50 to 100 nm | [46] |
| *Padina pavonica* Thivy and *Sargassum acinarium* Setchell 1933 extracts | $FeCl_3$ 0.1 M solution | Extract:precursor ratio 1:1, 60 min, room temperature, continuous stirring | Spherical $Fe_3O_4$ nanoparticles in the range of sizes 10 to 19.5 nm (*P. pavonica*) and 21.6 to 27.4 nm for *S. acinarium* | [47] |
| *Spirulina platensis* extracts | $FeCl_3 \cdot 6H_2O$ from 0.1 to 0.6 M | Extract:precursor ratio 1:1, immediate color change, stabilization for another 2 h at room temperature | Agglomerated non- uniform magnetic particles, diameter <10 nm | [98] |
| *Petalonia fascia*, *Colpomenia sinuosa* extracts | $FeCl_3.6H_2O$ (0.1 M) solution | Extract:precursor ratio 1:1, immediate color change, incubation for 72 h at room temperature | - spherical shape and size ranged from 6.54 to 13.46 nm with an average 9.42 ± 2.84 nm (*P. fascia)*<br>- cubic shape of the $Fe_3O_4$–NPs synthesized using *C. sinuosa* with a size range 10.56 to 19.91 nm and an average 17.78 ± 3.63 nm | [99] |
| *Sargassum muticum* extract | 0.1 M $FeCl_3$ solution | Extract:precursor ratio 1:1, immediate color change, the mixture was stirred for 60 min and then allowed to stand at room temperature for another 30 min | Cubic particles with mean diameter of 18 ± 4 nm | [57] |

**Table 2.** *Cont.*

| Algae | Precursor | Synthesis Conditions | Iron Nanoparticle Properties | Reference |
|---|---|---|---|---|
| *Chlorella vulgaris* extract | $FeCl_3.6H_2O$ | 15 min, continuous stirring, room temperature (controlled synthesis using algal extract and uncontrolled synthesis without algal extract) | Large aggregates of ultrafine nanoparticles obtained by uncontrolled synthesis, discrete spherical nanoparticles ranging from 8 to 17 nm for controlled synthesis in the presence of *C. vulgaris* secretory carbohydrates contained in the extract | [100] |
| *Enteromorpha* spp. extract | 0.1 M $FeCl_3$ solution | Extract was added drop by drop manually into 0.1 M $FeCl_3$ solution in a 1:2 volume ratio at room temperature, immediate color change | Spherical, porous agglomerates visible, mean diameter 78.83 nm | [101] |
| *Dictyota dicotoma* extract | $FeCl_3$ (2% solution) and $FeSO_4$ (1% solution) | Iron nanoparticles were prepared by adding ferric chloride (2%), ferrous sulphate (1%) solution, to the extracts (10 mL) and precipitated with 2 mL sodium hydroxide (0.1 M), pH 7–10, room temperature, 1 h, continuous stirring | Cubic nanoparticles, size range about 40 nm to 50 nm | [102] |
| *Moringa oleifera* extract | 0.6 M $FeCl_3$ solution | 80 mL of iron(III)chloride solution was mixed with 20 mL of the extract, 60 °C, 4h | Granular, homogenous, spherical-shaped structure with an average diameter of approximately 16 nm | [55] |

In direct comparison to the synthesis principle using plants, algal synthesis occurs in very much the same way: after extract preparation, precursor solutions are added, with a color change as an indicator of nanoparticle formation, which occurs almost instantaneously. Therefore, it can be concluded that this type of synthesis is also eco-friendly, fast, feasible and easy to perform.

### *5.3. Batch Synthesis Using Bacteria and Fungi*

Batch synthesis of iron nanoparticles using bacteria and fungi is also described in the literature as a sustainable, eco-friendly, adaptable and diverse method [31]. In comparison to synthesis that involves plant extracts, the procedure using fungi and bacteria is considered to be more complicated, mainly due to the fact that the biomass has to be grown and sustained prior to synthesis of iron nanoparticles, and the work has to be completed in aseptic conditions. Furthermore, the synthesis mechanisms can be intra- or extracellular, and, if the mechanisms are intracellular, there is an extra step in the separation of the iron nanoparticles: they first have to be excreted from the intracellular space to be further purified and used. In extracellular synthesis, metal ions are reduced to nanoparticles by microbial enzymes and proteins, bacterial or fungal cell wall components or organic molecules present in the culture medium. The intracellular process is connected to synthesis on the microbial wall; namely, the microbial wall contains carboxyl groups that are electrostatically charged and attract metal precursor ions that then pass the cell wall and enter the cell, where they are reduced by intracellular proteins and cofactors to nanoparticles [103]. Similar to biosynthesis using plant extracts, process conditions such as temperature, pH, biomass and others affect synthesis of iron nanoparticles, including the morphology, particle size distribution and yield of the synthesis.

Although bacteria are more commonly used in synthesizing nanoparticles, fungi could be more advantageous due to the presence of mycelia that provide greater surface area for interactions, but they also involve some risks, mostly related to biosafety, since some bacteria and fungi can be pathogenic [103]. The flowchart of synthesis is shown in Figure 3.

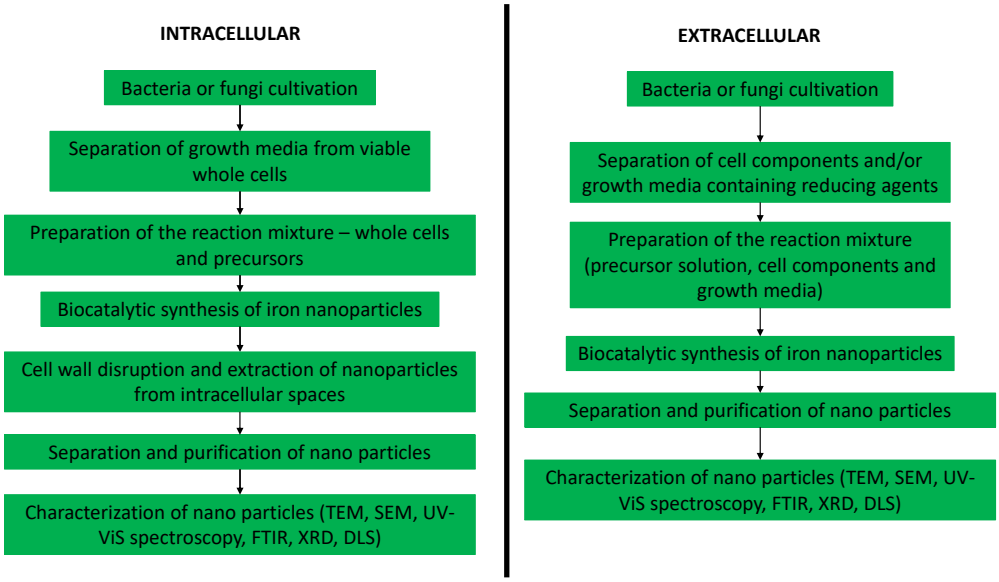


**Figure 3.** Flowchart of iron nanoparticle synthesis using bacteria and fungi.

An overview of some studies performed in the last several years involving green biosynthesis of INPs using bacteria and fungi is shown in Table 3.

**Table 3.** Some examples of use of bacteria and fungi for synthesis of iron nanoparticles.

| Microorganism | Precursor | Synthesis Conditions | Iron Nanoparticle Properties | Reference |
|---|---|---|---|---|
| Bacteria | | | | |
| *Bacillus megaterium* cell culture | 0.1 M $Fe(NO_3)_2$ solution | Bacterial suspensions combined with precursor solution at 1:1 ratio, room temperature, 20 min | Cubic shape, 40–60 nm | [104] |
| *Bacillus coagulans* (cell-free broth supernatant) | iron salt precursor $Fe^{3+}$ ($FeCl_3 \cdot 6H_2O$) and $Fe^{2+}$ ($FeCl_2 \cdot 4H_2O$) at a 2:1 M ratio | Cell-free broth supernatant was added to the precursor solution, 35 °C, 30 min, continuous stirring, pH = 11 | Irregular cubic shaped particles, diameter 4–33 nm | [105] |
| *Pseudomonas aeruginosa* (cell culture) | ferric quinate (FQ) solution | Intracellular synthesis, the isolates were cultured in a simple 9 K medium to isolate magnetotactic bacteria, magnetic properties confirmed by a magnet, magnetosomes extracted by sonication | Metallic structures, size 35–45 nm | [106] |
| *Actinobacter* spp. bacetrial biomass broth | $K_3Fe(CN)_6/K_4Fe(CN)_6$ mixture (2:1 molar ratio) | Bacterial biomass was cultured in a Luria broth, sterilized and, after 24 h, aqueous $K_3Fe(CN)_6/K_4Fe(CN)_6$ mixture (2:1 molar ratio) was added, 3 days, 150 rpm, 28 °C | After 24 h, quasi-spherical nanoparticles of 10−40 nm were obtained, after 48 h uniform cubic particles of 50−150 nm | [107] |
| *Magnetospirillum magneticum* culture broth | $FeCl_3$ | 29 °C, 24 h, 141 rpm, reaction mixture comprised of MTB culture and ferric chloride at different pH values (4–12) | Cuboidal and rectangular prisms, nearly spherical faceted nanoparticles, size 18–52 nm, depending on the pH of the mixture | [108] |
| *Streptomyces* sp. (SRT12) cell-free broth supernatant | $FeCl_2 \cdot 4H_2O$, $FeCl_3 \cdot 6H_2O$ | Cell-free supernatant was mixed with the precursor solution, 120 min, room temperature | Quasi-spherical, granular, crystalline and smooth cubical surfaced clusters with the size range from 65.0 to 86.7 nm | [109] |
| *Geobacter sulfurreducens* bacterial suspensions | FeO(OH), 50 mM | Cell cultures in deionized water containing an electron donor (sodium acetate 20 mM), an electron acceptor (Fe(III)-oxyhydroxide, 50 mM) and a sodium bicarbonate buffer (30 mM), 30 °C, 1 week incubation in the dark | Spherical and square shapes, particle size during synthesis can be controlled in the range 10–50 nm | [110] |
| *Proteus mirabilis* 10B bacterial suspensions | 7 mM of Fe $(NO_3)_3 \cdot 9H_2O$ | Proteus mirabilis 10B strain ($10^8$ CFU/mL) was inoculated to the optimized medium supplemented with 7 mM of Fe $(NO_3)_3 \cdot 9H_2O$; reaction was monitored based on color change of the reaction mixture | Uniform, small, monodispersed and spherical nanoparticles without distinct aggregation with a diameter of 1.44 to 1.92 nm; spider-web-like shape size 11.7 to 60.8 nm | [111] |

**Table 3.** *Cont.*

| Microorganism | Precursor | Synthesis Conditions | Iron Nanoparticle Properties | Reference |
|---|---|---|---|---|
| *Pseudomonas stutzeri* bacterial suspension | Ferric quinate (FQ) solution: 10 mM FQ solution was prepared by dissolving 0.27 g of ferric chloride and 0.19 g of quinic acid in 100 mL $H_2O$ | Bacterial culture was inoculated in 100 mL nutrient broth supplemented with 0.5 mM FQ. Of the two sets, one was incubated as static culture and other was agitated at 120 rpm at 37 °C for 72 h | Spherical in shape with rough surface. The mean diameter of IOMNPs clusters was estimated to be below 100 nm (SEM); spherical morphology with size in the range of 10–20 nm (TEM) | [112] |
| Fungi, yeasts | | | | |
| *Pennicillium roqeforti* fungal mycelia suspension | $FeCl_3 \cdot 6H_2O$, ferric chloride hexahydrate (0.001 M) and $FeCl_2 \cdot 4H_2O$ (0.001 mM) in the ratio 2:1 | 10 g of wet biomass was added to 90 mL mixture of salt solution and was incubated for 24 h at 28 °C in a dark-shaking incubator at 150 rpm | Non-spherical, coated, diameter 5–16 nm | [113] |
| *Saccharomyces cerevisiae yeast culture* suspended in a growth medium | $FeCl_3 \cdot 6H_2O$ (0.001 M), $FeSO_4 \cdot 7H_2O$ (0.1 M) | Freshly prepared yeast culture was added to the mixture of precursor solution, incubated in a rotary shaker at 30 °C at 120 rpm for 2–3 days | Spherical $Fe_2O_3$ particles, diameter 70–100 nm | [114] |
| *Alternaria alternata* (Mili-Q water cell-free filtrate) | $Fe(NO_3)_2$, 1 mM solution | Cell-free filtrate mixed with 1 mM $Fe(NO_3)_2$ incubated at 28 °C in dark with shaking (150 rpm) for 72 h | Cubic particles, diameter 5.4–12.1 nm | [37] |
| *Penicillium oxalicum* (Mili-Q water cell-free filtrate) | $FeSO_4$, 100 mM solution | Fungal mycelia filtrate was mixed with precursor solution (1:1), overnight, continuous stirring, 30 °C | Spherical shape, diameter 140 nm, agglomerates visible | [41] |
| *Aspergillus niger* homogenized mycelia cells solution | $FeSO_4$ and $FeCl_3$ solutions (2000 ppm) | Precursor/fungus solutions were incubated for 6 days at room temperature | Spherical particles synthesized intra- and extracellularly, Fe particles of 18 nm, $Fe_3O_4$ of 50 nm | [115] |
| *Trichoderma asperellum*, *Phialemoniopsis ocularis*, and *Fusarium incarnatum* fungal cell broth filtrate | $FeCl_3$ and $FeCl_2$ salt solution (2:1 mM final concentration) | Fungal cell filtrate mixed with $FeCl_3$ and $FeCl_2$ salt solution, 5 min, 30 °C, continuous stirring | Spherical with average particle size ranging between 25 ± 3.94 nm for *T. asperellum*, 13.13 ± 4.32 nm for *P. ocularis* and 30.56 ± 8.68 nm for *F. incarnatum* | [116] |
| *Aspergillus oryzae* TFR9 Mili-Q water cell-free filtrate | $FeCl_3$, 0.001 M solution | Cell-free filtrate and precursor solution were mixed and kept on rotary shaker at 28 °C at 150 rpm for 12 h | Spherical crystalline particles with diameters 10 nm and 24.6 nm | [117] |
| *Pleurotus florida* water extract | $FeCl_3$, 1 M solution | Mushroom extract:ferric chloride solution ratio 1:1, temperature 50–60°, stirred continuously | Spherical, roughly with 100 nm diameter | [118] |
| *Cryptococcus humicola* 9–6 cells suspended in a growth medium | $Fe_2SO_4 \cdot 7H_2O$, 0.05 M solution added to the growth medium | *C. humicola* nutrient media were enriched with iron, incubated at 22–25 °C, mixed every 3 days | Spherical nanoparticles present in the cell and adhered to the cell wall, diameter 8–9 nm | [119] |
| *Rhizopus stolonifera* (Mili-Q water cell-free filtrate) | $FeCl_3$, 1 mM solution | Cell filtrate(50 mL) was mixed with 50 mL of 1 M $FeCl_3$ solution, agitated in the orbital shaker for 72 h at room temperature | Diameter and morphology not determined in the study | [42] |

Based on the data shown in Table 3, different bacteria and fungi possess the ability to reduce precursor solutions of iron ions. All of them differ based on whether the synthesis occurs intra- or extracellularly, with the intracellular one being more complex because the nanoparticles have to be extracted from the cell to be further purified and used. Moreover, in direct comparison of fungal/bacterial and plant/algal synthesis, it can be noticed that the bacterial/fungal synthesis takes more time and requires specific incubation temperatures and times to be successful. Moreover, incubation of biomass and isolation of nanoparticles requires use of more chemicals, reagents and solvents, which makes this synthesis less feasible than the one using plants and algae.

## 6. Continuous Synthesis Using Microfluidic Systems

Surface-to-volume ratio (S/V) has dramatically increased with development of nanoscience and nanotechnology. Generally speaking, the majority of nanoparticles were created in a bulk system using traditional methods by changing the precursors into the desired NPs. According to Han and Jiang [120], there are some drawbacks of conventional batch techniques, which include polymerization, self-assembly and nanoprecipitation. Basic problems of functional NP synthesis are listed in the literature data as follows: (i) synthesis of nanoparticles is a laborious and challenging procedure, (ii) there is a good chance that the size distribution of nanoparticles is wide and (iii) lack of bulk fluidic control makes it challenging to create core-shell NPs. However, those issues can be avoided by creating functional NPs using microfluidic devices [121]. Due

to their high productivity, versatility, transparency, effectiveness, reproducibility and precision, microfluidic systems are excellent for synthesizing nanomaterials because they may be used to create multispecies strategies [122–124].

The advantages of using microfluidic systems include their compact size, low cost, need for few sample reagents, safe operation and user-friendly setting [125,126]. In a far more deliberate and regulated approach, microfluidics systems may produce uniform mixtures of particles [127–130]. In order to create NPs with greater quality optical, mechanical, biological and chemical characteristics for a variety of applications, researchers now rely on the miniature microfluidic platform [131,132]. Laminar fluid flow at the microscale size and considerably better heat/mass transmission are characteristics of microfluidics [133–135]. As described by James et al. [136], since the channels that make up microfluidic devices are so narrow, reaction conditions may be precisely controlled to provide uniform reaction volumes inside the channels. Furthermore, during coprecipitation of NPs, laminar flow provides great control over the kinetic characteristics of the two solutions to be combined. Microfluidic systems are mostly manufactured from chemically resistant materials, such as silicon, glass, thermoplastics, ceramics and metals, using (micro)fabrication, additive manufacturing and tubing/extrusion technologies [137]. Additionally, microfluidic technology has rapidly evolved to be one of the most important technologies in the field of purposive biomaterial production [138,139], along with the advantages of variable modification and large-scale integration.

### *6.1. Strategies for Iron Nanoparticle Synthesis Using Microfluidic Devices*

Due to the benefits already described, flow systems employed in nanosynthesis are now being researched extensively. Microfluidic systems can be categorized into two groups based on the phases they involve: single-phase continuous flow and segmented flow microfluidic systems [121,140]. As stated by James et al. [136], Niculescu et al. [140], Chen et al. [124] and Ma et al. [121], inverse mixing and reaction of various fluids within the microchannel is accomplished by continuous laminar flow in single-phase continuous flow microreactors. Geometric barriers can be inserted within the microchannels or the geometries of the microchannels can be altered to ensure appropriate mixing of the reactants. It is well-known that, in the laminar flow rate, dominant in a microfluidic device, molecule interdiffusion across laminar streams serves as the main mixing mechanism for passive mixers. Channel width and flow ratio of the miscible fluids are inversely correlated with mixing time [121]. As described by Abiev et al. [141], microreactors have shown to be the most effective tools for co-precipitation-based NP production, where micromixing can be enhanced by different diffusion path reduction approaches, such as: (i) using microinjector, (ii) using microreactor with swirled flows, (iii) application of microreactor with impinging swirled flow, (iv) using pulsating flow type apparatus, (iv) using straight axis two-phase microreactor, (v) injecting the flow into a main stream or (vi) injecting the substreams.

On the other hand, segmented flow microreactors and droplet microreactors are two categories of multiphase flow microreactors. They have numerous inlets and separate introductions of a gas and a liquid or a liquid and a liquid, forming a continuous and dispersive portion. The various reaction reagents are thoroughly combined and undergo chemical reactions in the dispersed portion. The fact that the reaction zone is not in contact with the outer channel walls is a benefit of the multiphase flow reactor, which significantly lowers the possibility of contamination and blockage of the microchannels. On the other hand, multiphase flow microreactor systems are difficult to manipulate and there is a possibility of reagent dispersion.

Under specific settings, it is possible to generate a consistent pattern of consecutive fluid slugs when two fluid flows (either immiscible liquids or a gas and a liquid) are injected in capillaries [142–145]. Meanwhile, the dispersion phase creates drops that are entirely captured by the continuous phase; the continuous phase makes slugs that are joined by thin films in interface with the tube walls [146,147]. The characteristics of the channel surface, specifically its wettability with regard to the two fluids, determine which phase is

continuous and which is disperse. The capillary number and the Weber number are the two primary dimensionless numbers that describe this flow [148,149]. Some examples of use of microfluidic systems for iron nanoparticle syntheses based on both approaches are provided in Table 4.

When optimizing NP production using microfluidic devices, different variables, such as volumetric flow rate, mixing efficiency, catalyst concentration, microchannel geometry and material and wall surface, play a significant role [150]. Suryawanshi et al. [151] compared the iron oxide NP synthesis in two geometries of continuous flow microreactors. It has been shown that different residence times and mixing behaviors noted in those systems have a significant impact on the polydispersion index and particle size of the produced iron oxide NPs, which in turn impact the stability and magnetic characteristics. An important factor to determine the mean particle size as well as the size distribution of NPs was found to be the reactant flow rate: as the reactant flow rate increased, the average particle size of iron oxide NPs dropped. Their results can be directly compared with those provided by Göpfert et al. [152]: magnetic iron NPs with average diameter of about 10 nm and low polydispersity index were synthesized using microfluidic technology. The effect of different ratios of iron ions and base iron ions at different flow rates on the process productivity was also analyzed. Ahrberg et al. [153] stated that, for the process of iron oxide NP synthesis using a droplet-based microfluidic device for short residence times (2–8 min), the influence of small differences in residence time on the mean particle diameter is rather considerable, and a direct correlation between the mean particle size and the residence time of the droplets in the reactor could be observed. However, as the reagent supply is decreased during extended residence intervals, the impact is reduced and the reaction is slowed.

One must take into account that gas–liquid processes are not well-studied in the aspect of production of nanomaterials. Panariello et al. [154] combined two modules and four distinct reactor systems were developed that enable control of the type of gas dissolved in the solution as well as the reactor flow pattern. Single-phase and liquid–liquid two-phase flows were analyzed. Optimization of temperature, flow pattern and dissolved gaseous reactants concentration enabled complete conversion of the iron precursor to magnetite/maghemite nanocrystals in just 3 min. The fluctuation in particle size distribution in the aforementioned studies suggests that the mean particle size is controlled by internal mixing, slip velocity and the physical characteristics of the fluids, and, most importantly, selection of the right inert phase will allow optimization for a wide range of particle size distributions. A similar conclusion was presented by Larrea et al. [155] involving the potential of using nitrogen, oxygen, hydrogen and carbon monoxide as the gas phase in lysine-$Fe_3O_4$ NP synthesis. The experiments were performed in a microfluidic set-up composed of two poly(tetrafluoroethylene) coils connected in series. The first one was used for mixing and the second one for the reaction. Their results showed that fast mixing is essential since nearly all the oxide precursors are removed from the liquid phase in less than a minute, leading to a fast nucleation process. They also stated that selection of the gas phase results in different morphologies and crystalline structures of nanoparticles.

**Table 4.** Some examples of use of microfluidic systems for nanoparticle syntheses.

| Nanoparticle | Microfluidic Device Geometry | Process Efficiency | Reference |
|---|---|---|---|
| Iron oxide core chitosan nanoparticles | 3D printed microchannel with T-shape inlet | With 20–120 mL/h flow rates and 0.06–0.03% concentrations at pH 4.5 for chitosan-tripolyphosphat, nanoparticles of diameter 190 ± 15 nm were obtained | [156] |
| Iron oxide nanoparticles | (Poly)tetrafluoro-ethylene (PTFE) tube microreactor with coaxial flows | Magnetic and stable colloidal iron oxide particles with a size less than 7 nm have been prepared | [157] |
| Superparamagnetic iron oxide nanoparticles | The experimental setup comprises two microreactors made of stainless steel lined up in succession. The reactor volume, which was 160 µL, was contained within microchannels that were 370 µm wide and 150 µm deep. | Residence time of 19.2 s resulted in a particle size distribution of 3.9 ± 0.9 nm | [158] |

### *6.2. Green Synthesis of Iron Nanoparticles Using Microfluidic Devices, Future Perspective and Research*

The basic advantages of microfluidic systems, such as their compact size, low cost, need for fewer sample reagents, safe operation and user-friendly setting [125,126], make them a green technology. The aim of green technologies and green chemistry is development of a process safe for the environment. Anastas and Warner [159] presented 12 principles of green chemistry to decrease or completely stop using dangerous substances and chemical processes:

(1) Waste reduction
(2) Atom economy during synthesis
(3) Less dangerous chemical synthesis
(4) Design of environmentally friendly chemicals
(5) Use of safer solvents
(6) Energy efficiency
(7) Use of chemicals made from renewable sources
(8) Reduced use of chemical derivatives
(9) Reduced use of catalysts
(10) Use of degradable chemicals
(11) Real-time monitoring of pollution
(12) Safe chemical procedures.

Therefore, application of environmentally friendly chemicals in microfluidic devices under mild operating conditions would fit the suggested green chemistry principles. However, use of environmentally friendly reagents in conjunction with microfluidic technology and low reaction temperatures for iron NP synthesis has not yet been thoroughly researched. Plant extracts and food grade molecules as biocatalysts used in microsystems have been studied for synthesis of zinc, silver and copper nanoparticles, with a noticeable lack of research on iron nanoparticles, which makes this area a very interesting one for future research. As described by Hang et al. [120], formation of nanoparticles benefits from the mixing processes, which can be performed in microchannels. As a result, the generated nanoparticles are consistent in size. Furthermore, it is also feasible to create complicated structures (such as core-shell, multilayer and so forth) on a single microfluidic chip. These distinct qualities make microfluidic iron nanoparticles ideal for application as therapeutic and diagnostic agents, imaging contrast agents, biosensors and drug delivery systems. However, the efficiency and quality monitoring of iron nanoparticles generated with the necessary features in terms of size and size distribution still need to be improved for continuous flow synthesis of nanoparticles with microreactors [160]. The lack of knowledge of the highly dynamic process, including fluidics, mass transfer/mixing and nanoprecipitation, especially in the early stages of the synthesis process, as well as comprehension of nucleation kinetics, are the main causes of production problems [161]. Furthermore, it is important to mention that special focus of the researchers should be put on use of environmentally friendly reagents in conjunction with microfluidic technology and low reaction temperatures according to green chemistry principles.

## 7. Conclusions

NP synthesis techniques and strategies have grown dramatically in recent years, with a change from the traditional batch-based method to the microfluidic platform. The increasing demand for development of more effective and environmentally friendly chemical processes is also evident in synthesis of nanoparticles, where heavy and toxic chemicals are being replaced with “green” chemicals. This work examined and summarized some recent work completed using both the traditional technique and the microfluidic strategy. It can be concluded that future developments in nanomaterial synthesis will focus on improving the green synthesis approach. The research will be focused on selection of the most efficient green catalysts as well as development of (micro)rector geometry that will ensure the highest process productivity.

**Author Contributions:** Conceptualization, M.B. and A.J.T.; methodology, M.B.; software, D.V.; writing—original draft preparation, M.B. and A.J.T.; writing—review and editing, T.J., D.V. and J.G.K.; visualization, T.J. All authors have read and agreed to the published version of the manuscript.

**Funding:** This research received no external funding.

**Data Availability Statement:** Not applicable.

**Conflicts of Interest:** The authors declare no conflict of interest.

## References

1. Som, C.; Berges, M.; Chaudhry, Q.; Dusinska, M.; Fernandes, T.F.; Olsen, S.I.; Nowack, B. The Importance of Life Cycle Concepts for the Development of Safe Nanoproducts. *Toxicology* **2010**, *269*, 160–169. [CrossRef] [PubMed]
2. Cushen, M.; Kerry, J.; Morris, M.; Cruz-Romero, M.; Cummins, E. Nanotechnologies in the Food Industry—Recent Developments, Risks and Regulation. *Trends Food Sci. Technol.* **2012**, *24*, 30–46. [CrossRef]
3. Koivisto, A.J.; Aromaa, M.; Mäkelä, J.M.; Pasanen, P.; Hussein, T.; Hämeri, K. Concept to Estimate Regional Inhalation Dose of Industrially Synthesized Nanoparticles. *ACS Nano* **2012**, *6*, 1195–1203. [CrossRef] [PubMed]
4. Mäkelä, J.M.; Keskinen, H.; Forsblom, T.; Keskinen, J. Generation of Metal and Metal Oxide Nanoparticles by Liquid Flame Spray Process. *J. Mater. Sci.* **2004**, *39*, 2783–2788. [CrossRef]
5. Savolainen, K.; Pylkkänen, L.; Norppa, H.; Falck, G.; Lindberg, H.; Tuomi, T.; Vippola, M.; Alenius, H.; Hämeri, K.; Koivisto, J.; et al. Nanotechnologies, Engineered Nanomaterials and Occupational Health and Safety—A Review. *Saf. Sci.* **2010**, *48*, 957–963. [CrossRef]
6. Vanlalveni, C.; Lallianrawna, S.; Biswas, A.; Selvaraj, M.; Changmai, B.; Rokhum, S.L. Green Synthesis of Silver Nanoparticles Using Plant Extracts and Their Antimicrobial Activities: A Review of Recent Literature. *RSC Adv.* **2021**, *11*, 2804–2837. [CrossRef]
7. Iravani, S.; Korbekandi, H.; Mirmohammadi, S.V.; Zolfaghari, B. Synthesis of Silver Nanoparticles: Chemical, Physical and Biological Methods. *Res. Pharm. Sci.* **2014**, *9*, 385–406.
8. Marquis, G.; Ramasamy, B.; Banwarilal, S.; Munusamy, A.P. Evaluation of Antibacterial Activity of Plant Mediated CaO Nanoparticles Using *Cissus quadrangularis* Extract. *J. Photochem. Photobiol. B Biol.* **2016**, *155*, 28–33. [CrossRef]
9. Kaur, M.; Chopra, D.S. Green Synthesis of Iron Nanoparticles for Biomedical Applications. *Glob. J. Nanomed.* **2018**, *4*, 68–77. [CrossRef]
10. Akintelu, S.A.; Oyebamiji, A.K.; Olugbeko, S.C.; Folorunso, A.S. Green Synthesis of Iron Oxide Nanoparticles for Biomedical Application and Environmental Remediation: A Review. *Eclet. Quim.* **2021**, *46*, 17–37. [CrossRef]
11. Cao, Y.; Dhahad, H.A.; El-Shorbagy, M.A.; Alijani, H.Q.; Zakeri, M.; Heydari, A.; Bahonar, E.; Slouf, M.; Khatami, M.; Naderifar, M.; et al. Green Synthesis of Bimetallic ZnO–CuO Nanoparticles and Their Cytotoxicity Properties. *Sci. Rep.* **2021**, *11*, 23479. [CrossRef] [PubMed]
12. Bharti, K.; Lone, S.A.; Singh, A.; Nathani, S.; Roy, P.; Sadhu, K.K. Green Synthesis of Luminescent Gold-Zinc Oxide Nanocomposites: Cell Imaging and Visible Light–Induced Dye Degradation. *Front. Chem.* **2021**, *9*, 105. [CrossRef]
13. Spanos, A.; Athanasiou, K.; Ioannou, A.; Fotopoulos, V.; Krasia-Christoforou, T. Functionalized Magnetic Nanomaterials in Agricultural Applications. *Nanomaterials* **2021**, *11*, 3106. [CrossRef]
14. Cao, M.; Li, Z.; Wang, J.; Ge, W.; Yue, T.; Li, R.; Colvin, V.L.; Yu, W.W. Food Related Applications of Magnetic Iron Oxide Nanoparticles: Enzyme Immobilization, Protein Purification, and Food Analysis. *Trends Food Sci. Technol.* **2012**, *27*, 47–56. [CrossRef]
15. Attia, N.F.; El-Monaem, E.M.A.; El-Aqapa, H.G.; Elashery, S.E.A.; Eltaweil, A.S.; El Kady, M.; Khalifa, S.A.M.; Hawash, H.B.; El-Seedi, H.R. Iron Oxide Nanoparticles and Their Pharmaceutical Applications. *Appl. Surf. Sci. Adv.* **2022**, *11*, 100284. [CrossRef]
16. Ebrahiminezhad, A.; Zare-Hoseinabadi, A.; Sarmah, A.K.; Taghizadeh, S.; Ghasemi, Y.; Berenjian, A. Plant-Mediated Synthesis and Applications of Iron Nanoparticles. *Mol. Biotechnol.* **2018**, *60*, 154–168. [CrossRef]
17. Mittal, A.K.; Chisti, Y.; Banerjee, U.C. Synthesis of Metallic Nanoparticles Using Plant Extracts. *Biotechnol. Adv.* **2013**, *31*, 346–356. [CrossRef] [PubMed]
18. Zhu, K.X.; Huang, S.; Peng, W.; Qian, H.F.; Zhou, H.M. Effect of Ultrafine Grinding on Hydration and Antioxidant Properties of Wheat Bran Dietary Fiber. *Food Res. Int.* **2010**, *43*, 943–948. [CrossRef]
19. Shibata, T. Method for Producing Green Tea in Microfine Powder. U.S. Patent No 6,416,803, 7 July 2002.
20. Brody, A.L.; Bugusu, B.; Han, J.H.; Sand, C.K.; McHugh, T.H. Innovative Food Packaging Solutions. *J. Food Sci.* **2008**, *73*, R107–R116. [CrossRef] [PubMed]
21. Jadoun, S.; Arif, R.; Jangid, N.K.; Meena, R.K. Green Synthesis of Nanoparticles Using Plant Extracts: A Review. *Environ. Chem. Lett.* **2021**, *19*, 355–374. [CrossRef]
22. Asghar, M.A.; Zahir, E.; Asghar, M.A.; Iqbal, J.; Rehman, A.A. Facile, One-Pot Biosynthesis and Characterization of Iron, Copper and Silver Nanoparticles Using *Syzygium cumini* Leaf Extract: As an Effective Antimicrobial and Aflatoxin B1 Adsorption Agents. *PLoS ONE* **2020**, *15*, e0234964. [CrossRef] [PubMed]
23. Machado, S.; Pinto, S.L.; Grosso, J.P.; Nouws, H.P.A.; Albergaria, J.T.; Delerue-Matos, C. Green Production of Zero-Valent Iron Nanoparticles Using Tree Leaf Extracts. *Sci. Total Environ.* **2013**, *445–446*, 1–8. [CrossRef] [PubMed]
24. Sozer, N.; Kokini, J.L. Nanotechnology and Its Applications in the Food Sector. *Trends Biotechnol.* **2009**, *27*, 82–89. [CrossRef]

25. Herlekar, M.; Barve, S.; Kumar, R. Plant-Mediated Green Synthesis of Iron Nanoparticles. *J. Nanoparticles* **2014**, *2014*, 1–9. [CrossRef]
26. Chauhan, S.; Upadhyay, L.S.B. Biosynthesis of Iron Oxide Nanoparticles Using Plant Derivatives of *Lawsonia inermis* (Henna) and Its Surface Modification for Biomedical Application. *Nanotechnol. Environ. Eng.* **2019**, *4*, 1–10. [CrossRef]
27. Batool, F.; Iqbal, M.S.; Khan, S.U.D.; Khan, J.; Ahmed, B.; Qadir, M.I. Biologically Synthesized Iron Nanoparticles (FeNPs) from *Phoenix dactylifera* Have Anti-Bacterial Activities. *Sci. Rep.* **2021**, *11*, 22132. [CrossRef]
28. Huber, D.L. Synthesis, Properties, and Applications of Iron Nanoparticles. *Small* **2005**, *1*, 482–501. [CrossRef]
29. Mahanty, S.; Bakshi, M.; Ghosh, S.; Gaine, T.; Chatterjee, S.; Bhattacharyya, S.; Das, S.; Das, P.; Chaudhuri, P. Mycosynthesis of Iron Oxide Nanoparticles Using Manglicolous Fungi Isolated from Indian Sundarbans and Its Application for the Treatment of Chromium Containing Solution: Synthesis, Adsorption Isotherm, Kinetics and Thermodynamics Study. *Environ. Nanotechnol. Monit. Manag.* **2019**, *12*, 100276. [CrossRef]
30. Ash, A.; Revati, K.; Pandey, B.D. Microbial Synthesis of Iron-Based Nanomaterials—A Review. *Bull. Mater. Sci.* **2011**, *34*, 191–198. [CrossRef]
31. Nadeem, M.; Khan, R.; Shah, N.; Bangash, I.R.; Abbasi, B.H.; Hano, C.; Liu, C.; Ullah, S.; Hashmi, S.S.; Nadhman, A.; et al. A Review of Microbial Mediated Iron Nanoparticles (IONPs) and Its Biomedical Applications. *Nanomaterials* **2022**, *12*, 130. [CrossRef]
32. Kianpour, S.; Ebrahiminezhad, A.; Deyhimi, M.; Negahdaripour, M.; Raee, M.J.; Mohkam, M.; Rezaee, H.; Irajie, C.; Berenjian, A.; Ghasemi, Y. Structural Characterization of Polysaccharide-Coated Iron Oxide Nanoparticles Produced by *Staphylococcus warneri*, Isolated from a Thermal Spring. *J. Basic Microbiol.* **2019**, *59*, 569–578. [CrossRef] [PubMed]
33. Sundaram, P.A.; Augustine, R.; Kannan, M. Extracellular Biosynthesis of Iron Oxide Nanoparticles by Bacillus Subtilis Strains Isolated from *Rhizosphere soil*. *Biotechnol. Bioprocess Eng.* **2012**, *17*, 835–840. [CrossRef]
34. Arias, S.L.; Shetty, A.R.; Senpan, A.; Echeverry-Rendón, M.; Reece, L.M.; Allain, J.P. Fabrication of a Functionalized Magnetic Bacterial Nanocellulose with Iron Oxide Nanoparticles. *J. Vis. Exp.* **2016**, *2016*, e52951. [CrossRef]
35. Fani, M.; Ghandehari, F.; Rezaee, M. Biosynthesis of Iron Oxide Nanoparticles by Cytoplasmic Extract of Bacteria *Lactobacillus fermentum*. *J. Med. Chem. Sci.* **2018**, *1*, 28–30.
36. Kaur, K.; Sidhu, A.K. Green Synthesis: An Eco-Friendly Route for the Synthesis of Iron Oxide Nanoparticles. *Front. Nanotechnol.* **2021**, *3*, 47.
37. Mohamed, Y.M.; Azzam, A.M.; Amin, B.H.; Safwat, N.A. Mycosynthesis of Iron Nanoparticles by *Alternaria alternata* and Its Antibacterial Activity. *Afr. J. Biotechnol.* **2015**, *14*, 1234–1241. [CrossRef]
38. Sidkey, N. Biosynthesis, Characterization and Antimicrobial Activity of Iron Oxide Nanoparticles Synthesized by Fungi. *Al-Azhar J. Pharm. Sci.* **2020**, *62*, 164–179. [CrossRef]
39. Baskar, G.; Chandhuru, J.; Praveen, A.S.; Sheraz Fahad, K. Anticancer Activity of Iron Oxide Nanobiocomposite of Fungal *Asparaginase*. *Int. J. Mod. Sci. Technol.* **2017**, *2*, 98–104.
40. Baccile, N.; Noiville, R.; Stievano, L.; Bogaert, I. Van Sophorolipids-Functionalized Iron Oxide Nanoparticles. *Phys. Chem. Chem. Phys.* **2013**, *15*, 1606–1620. [CrossRef]
41. Mathur, P.; Saini, S.; Paul, E.; Sharma, C.; Mehtani, P. Endophytic Fungi Mediated Synthesis of Iron Nanoparticles: Characterization and Application in Methylene Blue Decolorization. *Curr. Res. Green Sustain. Chem.* **2021**, *4*, 100053. [CrossRef]
42. Adeleye, T.M.; Kareem, S.O.; Kekere-Ekun, A.A. Optimization Studies on Biosynthesis of Iron Nanoparticles Using Rhizopus stolonifer. In Proceedings of the IOP Conference Series: Materials Science and Engineering, Ulaanbaatar, Mongolia, 10–13 September 2020; Volume 805.
43. Arya, A.; Chundawat, T.S. Metal Nanoparticles from Algae: A Green Approach for the Synthesis, Characterization and Their Biological Activity. *Nanosci. Nanotechnol.-Asia* **2018**, *10*, 185–202. [CrossRef]
44. LewisOscar, F.; Vismaya, S.; Arunkumar, M.; Thajuddin, N.; Dhanasekaran, D.; Nithya, C. Algal Nanoparticles: Synthesis and Biotechnological Potentials. In *Algae—Organisms for Imminent Biotechnology*; Books on Demand GmbH: Hamburg, Germany, 2016.
45. Taghizadeh, S.; Taherpoor, A.; Ebrahiminezhad, A. Review Paper: Algae and Microalgae Mediated Synthesis of Iron Nanoparticles and Their Applications. *JAMSAT* **2020**, *5*, 1–11.
46. Win, T.T.; Khan, S.; Bo, B.; Zada, S.; Fu, P.C. Green Synthesis and Characterization of $Fe_3O_4$ Nanoparticles Using *Chlorella*-K01 Extract for Potential Enhancement of Plant Growth Stimulating and Antifungal Activity. *Sci. Rep.* **2021**, *11*, 21996. [CrossRef] [PubMed]
47. El-Kassas, H.Y.; Aly-Eldeen, M.A.; Gharib, S.M. Green Synthesis of Iron Oxide ($Fe_3O_4$) Nanoparticles Using Two Selected Brown Seaweeds: Characterization and Application for Lead Bioremediation. *Acta Oceanol. Sin.* **2016**, *35*, 89–98. [CrossRef]
48. Salem, D.M.S.A.; Ismail, M.M.; Tadros, H.R.Z. Evaluation of the Antibiofilm Activity of Three Seaweed Species and Their Biosynthesized Iron Oxide Nanoparticles ($Fe_3O_4$-NPs). *Egypt. J. Aquat. Res.* **2020**, *46*, 333–339. [CrossRef]
49. Mukherjee, A.; Sarkar, D.; Sasmal, S. A Review of Green Synthesis of Metal Nanoparticles Using Algae. *Front. Microbiol.* **2021**, *12*, 693899. [CrossRef] [PubMed]
50. Puthukkara, A.R.P.; Jose, S.T.; Lal, D.S. Plant Mediated Synthesis of Zero Valent Iron Nanoparticles and Its Application in Water Treatment. *J. Environ. Chem. Eng.* **2021**, *9*, 104569. [CrossRef]
51. AL-Husseini, A.H.; Sih, B.T.; Al-Araji, A.M. Green Synthesis of Iron Oxide Nanoparticles ($Fe_2O_3$) Using Saffron Extract. *Proc. J. Phys. Conf. Ser.* **2021**, *2114*, 012082. [CrossRef]

52. Groiss, S.; Selvaraj, R.; Varadavenkatesan, T.; Vinayagam, R. Structural Characterization, Antibacterial and Catalytic Effect of Iron Oxide Nanoparticles Synthesised Using the Leaf Extract of *Cynometra ramiflora*. *J. Mol. Struct.* **2017**, *1128*, 572–578. [CrossRef]
53. Jagtap, U.R.; Bapat, V.A. Green synthesis of silver nanoparticles using *Artocarpus heterophyllus* Lam. seed extract and its antibacterial activity. *Ind. Crops Prod.* **2013**, *46*, 132–137. [CrossRef]
54. Kanagasubbulakshmi, S.; Kadirvelu, K. Green Synthesis of Iron Oxide Nanoparticles Using *Lagenaria siceraria* and Evaluation of Its Antimicrobial Activity. *Def. Life Sci. J.* **2017**, *2*, 422. [CrossRef]
55. Kiwumulo, H.F.; Muwonge, H.; Ibingira, C.; Lubwama, M.; Kirabira, J.B.; Ssekitoleko, R.T. Green Synthesis and Characterization of Iron-Oxide Nanoparticles Using *Moringa oleifera*: A Potential Protocol for Use in Low and Middle Income Countries. *BMC Res. Notes* **2022**, *15*, 149. [CrossRef] [PubMed]
56. Gottimukkala, K. Green Synthesis of Iron Nanoparticles Using Green Tea Leaves Extract. *J. Nanomedine. Biother. Discov.* **2017**, *7*, 1000151. [CrossRef]
57. Mahdavi, M.; Namvar, F.; Ahmad, M.B.; Mohamad, R. Green Biosynthesis and Characterization of Magnetic Iron Oxide ($Fe_3O_4$) Nanoparticles Using Seaweed (*Sargassum muticum*) Aqueous Extract. *Molecules* **2013**, *18*, 5954–5964. [CrossRef]
58. Mirza, A.U.; Kareem, A.; Nami, S.A.A.; Khan, M.S.; Rehman, S.; Bhat, S.A.; Mohammad, A.; Nishat, N. Biogenic Synthesis of Iron Oxide Nanoparticles Using *Agrewia optiva* and *Prunus persica* Phyto Species: Characterization, Antibacterial and Antioxidant Activity. *J. Photochem. Photobiol. B Biol.* **2018**, *185*, 262–274. [CrossRef]
59. Shahwan, T.; Abu Sirriah, S.; Nairat, M.; Boyaci, E.; Eroğlu, A.E.; Scott, T.B.; Hallam, K.R. Green Synthesis of Iron Nanoparticles and Their Application as a Fenton-like Catalyst for the Degradation of Aqueous Cationic and Anionic Dyes. *Chem. Eng. J.* **2011**, *172*, 258–266. [CrossRef]
60. Thacker, H.H.; Ram, V.R.; Dave, P.N. Plant Mediated Synthesis of Iron Nanoparticles and Their Applications: A Review. *Prog. Chem. Biochem. Res.* **2019**, *2*, 84–91. [CrossRef]
61. Majumdar, M.; Khan, S.A.; Nandi, N.B.; Roy, S.; Panja, A.S.; Roy, D.N.; Misra, T.K. Green Synthesis of Iron Nanoparticles for Investigation of Biofilm Inhibition Property. *ChemistrySelect* **2020**, *5*, 13575–13583. [CrossRef]
62. Karunakaran, S.; Ramanujam, S.; Gurunathan, B. Green Synthesised Iron and Iron-Based Nanoparticle in Environmental and Biomedical Application: A Review. *IET Nanobiotechnol.* **2018**, *12*, 1003–1008. [CrossRef] [PubMed]
63. Huang, L.; Weng, X.; Chen, Z.; Megharaj, M.; Naidu, R. Green Synthesis of Iron Nanoparticles by Various Tea Extracts: Comparative Study of the Reactivity. *Spectrochim. Acta. A Mol. Biomol. Spectrosc.* **2014**, *130*, 295–301. [CrossRef]
64. Harshiny, M.; Iswarya, C.N.; Matheswaran, M. Biogenic Synthesis of Iron Nanoparticles Using *Amaranthus dubius* Leaf Extract as a Reducing Agent. *Powder Technol.* **2015**, *286*, 744–749. [CrossRef]
65. Martínez-Cabanas, M.; López-García, M.; Barriada, J.L.; Herrero, R.; Sastre de Vicente, M.E. Green Synthesis of Iron Oxide Nanoparticles. Development of Magnetic Hybrid Materials for Efficient As(V) Removal. *Chem. Eng. J.* **2016**, *301*, 83–91. [CrossRef]
66. Lenders, J.J.M.; Mirabello, G.; Sommerdijk, N.A.J.M. Bioinspired Magnetite Synthesis via Solid Precursor Phases. *Chem. Sci.* **2016**, *7*, 5624–5634. [CrossRef]
67. Woźnica, A.; Dzirba, J.; Mańka, D.; Łabuzek, S. Effects of Electron Transport Inhibitors on Iron Reduction in *Aeromonas hydrophila* Strain KB1. *Anaerobe* **2003**, *9*, 125–130. [CrossRef] [PubMed]
68. Huang, L.; Luo, F.; Chen, Z.; Megharaj, M.; Naidu, R. Green Synthesized Conditions Impacting on the Reactivity of Fe NPs for the Degradation of Malachite Green. *Spectrochim. Acta Part A Mol. Biomol. Spectrosc.* **2015**, *137*, 154–159. [CrossRef]
69. Nadagouda, M.N.; Castle, A.B.; Murdock, R.C.; Hussain, S.M.; Varma, R.S. In Vitro Biocompatibility of Nanoscale Zerovalent Iron Particles (NZVI) Synthesized Using Tea Polyphenols. *Green Chem.* **2010**, *12*, 114–122. [CrossRef]
70. Saranya, S.; Vijayarani, K.; Pavithra, S. Green Synthesis of Iron Nanoparticles Using Aqueous Extract of *Musa ornata* Flower Sheath against Pathogenic Bacteria. *Indian J. Pharm. Sci.* **2017**, *79*, 688–694. [CrossRef]
71. Yehia, R.S.; Ali, A.M. Biosynthesis and Characterization of Iron Nanoparticles Produced by *Thymus vulgaris* L. And Their Antimicrobial Activity. *Acta Bot. Croat.* **2020**, *77*, 114–120. [CrossRef]
72. Ehrampoush, M.H.; Miria, M.; Salmani, M.H.; Mahvi, A.H. Cadmium Removal from Aqueous Solution by Green Synthesis Iron Oxide Nanoparticles with Tangerine Peel Extract. *J. Environ. Health Sci. Eng.* **2015**, *13*, 84. [CrossRef] [PubMed]
73. Muthukumar, H.; Matheswaran, M. *Amaranthus spinosus* Leaf Extract Mediated FeO Nanoparticles: Physicochemical Traits, Photocatalytic and Antioxidant Activity. *ACS Sustain. Chem. Eng.* **2015**, *3*, 3149–3156. [CrossRef]
74. Patra, J.K.; Baek, K.H. Green Biosynthesis of Magnetic Iron Oxide ($Fe_3O_4$) Nanoparticles Using the Aqueous Extracts of Food Processing Wastes under Photo-Catalyzed Condition and Investigation of Their Antimicrobial and Antioxidant Activity. *J. Photochem. Photobiol. B Biol.* **2017**, *173*, 291–300. [CrossRef] [PubMed]
75. Rajendran, K.; Sen, S. Optimization of Process Parameters for the Rapid Biosynthesis of Hematite Nanoparticles. *J. Photochem. Photobiol. B Biol.* **2016**, *159*, 82–87. [CrossRef] [PubMed]
76. Bibi, I.; Nazar, N.; Ata, S.; Sultan, M.; Ali, A.; Abbas, A.; Jilani, K.; Kamal, S.; Sarim, F.M.; Khan, M.I.; et al. Green Synthesis of Iron Oxide Nanoparticles Using Pomegranate Seeds Extract and Photocatalytic Activity Evaluation for the Degradation of Textile Dye. *J. Mater. Res. Technol.* **2019**, *8*, 6115–6124. [CrossRef]
77. Khan, S.; Bibi, G.; Dilbar, S.; Iqbal, A.; Ahmad, M.; Ali, A.; Ullah, Z.; Jaremko, M.; Iqbal, J.; Ali, M.; et al. Biosynthesis and Characterization of Iron Oxide Nanoparticles from *Mentha spicata* and Screening Its Combating Potential against Phytophthora Infestans. *Front. Plant Sci.* **2022**, *13*, 1001499. [CrossRef]

78. Sayed, F.N.; Polshettiwar, V. Facile and Sustainable Synthesis of Shaped Iron Oxide Nanoparticles: Effect of Iron Precursor Salts on the Shapes of Iron Oxides. *Sci. Rep.* **2015**, *5*, 9733. [CrossRef]
79. Verma, A.; Mehata, M.S. Controllable Synthesis of Silver Nanoparticles Using Neem Leaves and Their Antimicrobial Activity. *J. Radiat. Res. Appl. Sci.* **2016**, *9*, 109–115. [CrossRef]
80. Madivoli, E.S.; Kareru, P.G.; Maina, E.G.; Nyabola, A.O.; Wanakai, S.I.; Nyang'au, J.O. Biosynthesis of Iron Nanoparticles Using *Ageratum conyzoides* Extracts, Their Antimicrobial and Photocatalytic Activity. *SN Appl. Sci.* **2019**, *1*, 500. [CrossRef]
81. Lakshmnarayanan, S.; Shereen, M.F.; Niraimathi, K.L.; Brindha, P.; Arumugam, A. One-Pot Green Synthesis of Iron Oxide Nanoparticles from *Bauhinia tomentosa*: Characterization and Application towards Synthesis of 1, 3 Diolein. *Sci. Rep.* **2021**, *11*, 8643. [CrossRef]
82. Bhuiyan, M.S.H.; Miah, M.Y.; Paul, S.C.; Aka, T.D.; Saha, O.; Rahaman, M.M.; Sharif, M.J.I.; Habiba, O.; Ashaduzzaman, M. Green Synthesis of Iron Oxide Nanoparticle Using *Carica papaya* Leaf Extract: Application for Photocatalytic Degradation of Remazol Yellow RR Dye and Antibacterial Activity. *Heliyon* **2020**, *6*, e04603. [CrossRef]
83. Devi, H.S.; Boda, M.A.; Shah, M.A.; Parveen, S.; Wani, A.H. Green Synthesis of Iron Oxide Nanoparticles Using *Platanus orientalis* Leaf Extract for Antifungal Activity. *Green Process. Synth.* **2019**, *8*, 38–45. [CrossRef]
84. Buarki, F.; AbuHassan, H.; Al Hannan, F.; Henari, F.Z. Green Synthesis of Iron Oxide Nanoparticles Using *Hibiscus rosa* Sinensis Flowers and Their Antibacterial Activity. *J. Nanotechnol.* **2022**, *2022*, 5474645. [CrossRef]
85. Jain, R.; Mendiratta, S.; Kumar, L.; Srivastava, A. Green Synthesis of Iron Nanoparticles Using *Artocarpus heterophyllus* Peel Extract and Their Application as a Heterogeneous Fenton-like Catalyst for the Degradation of Fuchsin Basic Dye. *Curr. Res. Green Sustain. Chem.* **2021**, *4*, 100086. [CrossRef]
86. Kamath, V.; Chandra, P.; Jeppu, G.P. Comparative Study of Using Five Different Leaf Extracts in the Green Synthesis of Iron Oxide Nanoparticles for Removal of Arsenic from Water. *Int. J. Phytoremed.* **2020**, *22*, 1278–1294. [CrossRef]
87. Nahari, M.H.; Al Ali, A.; Asiri, A.; Mahnashi, M.H.; Shaikh, I.A.; Shettar, A.K.; Hoskeri, J. Green Synthesis and Characterization of Iron Nanoparticles Synthesized from Aqueous Leaf Extract of *Vitex leucoxylon* and Its Biomedical Applications. *Nanomaterials* **2022**, *12*, 2404. [CrossRef]
88. Truskewycz, A.; Shukla, R.; Ball, A.S. Phytofabrication of Iron Nanoparticles for Hexavalent Chromium Remediation. *ACS Omega* **2018**, *3*, 10781–10790. [CrossRef]
89. Jafer Aziz, W.; Abd Urabe, A. Chemical Preparation of Iron Oxide Nanoparticles Using Plants Extracts in Antibacterial Application. *Int. J. Bioorganic Chem.* **2019**, *4*, 1–6. [CrossRef]
90. Üstün, E.; Önbaş, S.C.; Kübra Çelik, S.; Çol Ayvaz, M.; Şahin, N. Green Synthesis of Iron Oxide Nanoparticles by Using *Ficus carica* Leaf Extract and Its Antioxidant Activity. *Biointerface Res. Appl. Chem.* **2022**, *12*, 2108–2116. [CrossRef]
91. Syarifah, S.; Imawan, C.; Handayani, W.; Djuhana, D. Biosynthesis of Ferric Oxide Nanoparticles Using *Pometia pinnata* J.R. Frost. & G.Forst. Leaves Water Extract. *Proc. AIP Conf. Proc.* **2018**, *2023*, 20054. [CrossRef]
92. Yusefi, M.; Shameli, K.; Yee, O.S.; Teow, S.Y.; Hedayatnasab, Z.; Jahangirian, H.; Webster, T.J.; Kuča, K. Green Synthesis of Fe3O4 Nanoparticles Stabilized by a *Garcinia mangostana* Fruit Peel Extract for Hyperthermia and Anticancer Activities. *Int. J. Nanomed.* **2021**, *16*, 2515–2532. [CrossRef]
93. Prabhu, N.N.; Kowshik, M. Green Route Synthesis and Preliminary Characterization of Iron Oxide Nanoparticles Using Leaf Extract of *Ocimum tenuiflorum*. *Adv. Mater. Sci. Eng.* **2019**, *3*. [CrossRef]
94. Pallela, P.N.V.K.; Ummey, S.; Ruddaraju, L.K.; Gadi, S.; Cherukuri, C.S.L.; Barla, S.; Pammi, S.V.N. Antibacterial Efficacy of Green Synthesized α-$Fe_2O_3$ Nanoparticles Using *Sida cordifolia* Plant Extract. *Heliyon* **2019**, *5*, e02765. [CrossRef]
95. Parajuli, K.; Sah, A.K.; Paudyal, H.; Parajuli, K.; Sah, A.K.; Paudyal, H. Green Synthesis of Magnetite Nanoparticles Using Aqueous Leaves Extracts of *Azadirachta indica* and Its Application for the Removal of As(V) from Water. *Green Sustain. Chem.* **2020**, *10*, 117–132. [CrossRef]
96. Bensy, A.D.V.; Christobel, G.J.; Muthusamy, K.; Alfarhan, A.; Anantharaman, P. Green Synthesis of Iron Nanoparticles from *Ulva lactuca* and Bactericidal Activity against Enteropathogens. *J. King Saud Univ. Sci.* **2022**, *34*, 101888. [CrossRef]
97. Salem, D.M.S.A.; Ismail, M.M.; Aly-Eldeen, M.A. Biogenic Synthesis and Antimicrobial Potency of Iron Oxide ($Fe_3O_4$) Nanoparticles Using Algae Harvested from the Mediterranean Sea, Egypt. *Egypt. J. Aquat. Res.* **2019**, *45*, 197–204. [CrossRef]
98. Shalaby, S.M.; Madkour, F.F.; El-Kassas, H.Y.; Mohamed, A.A.; Elgarahy, A.M. Green Synthesis of Recyclable Iron Oxide Nanoparticles Using *Spirulina platensis* Microalgae for Adsorptive Removal of Cationic and Anionic Dyes. *Environ. Sci. Pollut. Res.* **2021**, *28*, 65549–65572. [CrossRef]
99. El-Sheekh, M.M.; El-Kassas, H.Y.; Shams El-Din, N.G.; Eissa, D.I.; El-Sherbiny, B.A. Green Synthesis, Characterization Applications of Iron Oxide Nanoparticles for Antialgal and Wastewater Bioremediation Using Three Brown Algae. *Int. J. Phytoremed.* **2021**, *23*, 1538–1552. [CrossRef]
100. Ghanbariasad, A.; Taghizadeh, S.M.; Show, P.L.; Nomanbhay, S.; Berenjian, A.; Ghasemi, Y.; Ebrahiminezhad, A. Controlled Synthesis of Iron Oxyhydroxide (FeOOH) Nanoparticles Using Secretory Compounds from *Chlorella vulgaris* Microalgae. *Bioengineered* **2019**, *10*, 390–396. [CrossRef]
101. Ercan, G.; Uzunoğlu, D.; Ergüt, M.; Özer, A. Biosynthesis and Characterization of Iron Oxide Nanoparticles from *Enteromorpha* spp. Extract: Determination of Adsorbent Properties for Copper (II) Ions. *Int. Adv. Res. Eng. J.* **2019**, *3*, 65–74.
102. Chandran, M.; Yuvaraj, D.; Christudhas, L.; Kv, R. Bio-Synthesis of Iron Nanoparticles Using the Brown Seaweed, *Dictyota dicotoma*. *Biotechnol.* **2016**, *12*, 5–9.

103. Lahiri, D.; Nag, M.; Sheikh, H.I.; Sarkar, T.; Edinur, H.A.; Pati, S.; Ray, R.R. Microbiologically-Synthesized Nanoparticles and Their Role in Silencing the Biofilm Signaling Cascade. *Front. Microbiol.* **2021**, *12*, 180. [CrossRef]
104. Ghani, S.; Rafiee, B.; Sadeghi, D.; Ahsani, M. Biosynthesis of Iron Nano-Particles by *Bacillus megaterium* and Its Anti-Bacterial Properties. *J. Babol. Univ. Med. Sci.* **2017**, *19*, 13–19. [CrossRef]
105. Al-Maliki, Q.A.; Taj-Aldeen, W.R. Antibacterial and Antibiofilm Activity of Bacteria Mediated Synthesized $Fe_3O_4$ Nanoparticles Using *Bacillus coagulans*. *J. Nanostruct.* **2021**, *11*, 782–789. [CrossRef]
106. Khan, A.A.; Khan, S.; Khan, S.; Rentschler, S.; Laufer, S.; Deigner, H.P. Biosynthesis of Iron Oxide Magnetic Nanoparticles Using Clinically Isolated *Pseudomonas aeruginosa*. *Sci. Rep.* **2021**, *11*, 20503. [CrossRef]
107. Bharde, A.; Wani, A.; Shouche, Y.; Joy, P.A.; Prasad, B.L.V.; Sastry, M. Bacterial Aerobic Synthesis of Nanocrystalline Magnetite. *J. Am. Chem. Soc.* **2005**, *127*, 9326–9327. [CrossRef]
108. Obayemi, J.D.; Dozie-Nwachukwu, S.; Danyuo, Y.; Odusanya, O.S.; Anuku, N.; Malatesta, K.; Soboyejo, W.O. Biosynthesis and the Conjugation of Magnetite Nanoparticles with Luteinizing Hormone Releasing Hormone (LHRH). *Mater. Sci. Eng. C* **2015**, *46*, 482–496. [CrossRef]
109. Rajeswaran, S.; Somasundaram Thirugnanasambandan, S.; Dewangan, N.K.; Moorthy, R.K.; Kandasamy, S.; Vilwanathan, R. Multifarious Pharmacological Applications of Green Routed Eco-Friendly Iron Nanoparticles Synthesized by *Streptomyces* sp. (SRT12). *Biol. Trace Elem. Res.* **2020**, *194*, 273–283. [CrossRef]
110. Byrne, J.M.; Telling, N.D.; Coker, V.S.; Pattrick, R.A.D.; Van Der Laan, G.; Arenholz, E.; Tuna, F.; Lloyd, J.R. Control of Nanoparticle Size, Reactivity and Magnetic Properties during the Bioproduction ofmagnetite by *Geobacter sulfurreducens*. *Nanotechnology* **2011**, *22*, 455709. [CrossRef]
111. Zaki, S.A.; Eltarahony, M.M.; Abd-El-Haleem, D.A. Disinfection of Water and Wastewater by Biosynthesized Magnetite and Zerovalent Iron Nanoparticles via NAP-NAR Enzymes of *Proteus mirabilis* 10B. *Environ. Sci. Pollut. Res.* **2019**, *26*, 23661–23678. [CrossRef]
112. Desai, M.P.; Pawar, K.D. Immobilization of Cellulase on Iron Tolerant *Pseudomonas stutzeri* Biosynthesized Photocatalytically Active Magnetic Nanoparticles for Increased Thermal Stability. *Mater. Sci. Eng. C* **2020**, *106*, 110169. [CrossRef]
113. Ali, A.T.; Elewa, N.; Elbostany, N.A.; Shetaia, Y.M.; Swilm, M. Antimicrobial Potentiality of Green Synthesized Iron Oxide Nanoparticles by *Penicillium roqueforti*. *Egy. J. Pure Appl. Sci* **2021**, *59*, 29–43. [CrossRef]
114. Asha Ranjani, V.; Tulja Rani, G.; Sowjanya, M.; Preethi, M.; Srinivas, M.; Nikhil, M. Yeast Mediated Synthesis of Iron Oxide Nano Particles: Its Characterization and Evaluation of Antibacterial Activity. *Int. Res. J. Pharm. Med. Sci.* **2022**, *5*, 12–16.
115. Abdeen, M.; Sabry, S.; Ghozlan, H.; El-Gendy, A.A.; Carpenter, E.E. Microbial-Physical Synthesis of Fe and $Fe_3O_4$ Magnetic Nanoparticles Using *Aspergillus niger* YESM1 and Supercritical Condition of Ethanol. *J. Nanomater.* **2016**, *2016*, 9174891. [CrossRef]
116. Mahanty, S.; Bakshi, M.; Ghosh, S.; Chatterjee, S.; Bhattacharyya, S.; Das, P.; Das, S.; Chaudhuri, P. Green Synthesis of Iron Oxide Nanoparticles Mediated by Filamentous Fungi Isolated from Sundarban Mangrove Ecosystem, India. *Bionanoscience* **2019**, *9*, 637–651. [CrossRef]
117. Tarafdar, J.C.; Raliya, R. Rapid, Low-Cost, and Ecofriendly Approach for Iron Nanoparticle Synthesis Using *Aspergillus oryzae* TFR9. *J. Nanopart.* **2013**, *2013*, 141274. [CrossRef]
118. Manikandan, G.; Ramasubbu, R. Biosynthesis of Iron Nanoparticles from Pleurotus Florida and Its Antimicrobial Activity against Selected Human Pathogens. *Indian J. Pharm. Sci.* **2021**, *83*, 45–51. [CrossRef]
119. Vainshtein, M.; Belova, N.; Kulakovskaya, T.; Suzina, N.; Sorokin, V. Synthesis of Magneto-Sensitive Iron-Containing Nanoparticles by Yeasts. *J. Ind. Microbiol. Biotechnol.* **2014**, *41*, 657–663. [CrossRef]
120. Han, Z.; Jiang, X. Microfluidic Synthesis of Functional Nanoparticles. *Nanotechnol. Microfluid.* **2020**. [CrossRef]
121. Ma, J.; Lee, S.M.Y.; Yi, C.; Li, C.W. Controllable Synthesis of Functional Nanoparticles by Microfluidic Platforms for Biomedical Applications-a Review. *Lab Chip* **2017**, *17*, 209–226. [CrossRef]
122. Frey, N.; Sönmez, U.M.; Minden, J.; LeDuc, P. Microfluidics for Understanding Model Organisms. *Nat. Commun.* **2022**, *13*, 3195. [CrossRef]
123. Nielsen, J.B.; Hanson, R.L.; Almughamsi, H.M.; Pang, C.; Fish, T.R.; Woolley, A.T. Microfluidics: Innovations in Materials and Their Fabrication and Functionalization. *Anal. Chem.* **2020**, *92*, 150. [CrossRef]
124. Chen, Z.; Lv, Z.; Zhang, Z.; Weitz, D.A.; Zhang, H.; Zhang, Y.; Cui, W. Advanced Microfluidic Devices for Fabricating Multi-Structural Hydrogel Microsphere. *Exploration* **2021**, *1*, 20210036. [CrossRef]
125. Fong, E.J.; Huang, C.; Hamilton, J.; Benett, W.J.; Bora, M.; Burklund, A.; Metz, T.R.; Shusteff, M. A Microfluidic Platform for Precision Small-Volume Sample Processing and Its Use to Size Separate Biological Particles with an Acoustic Microdevice. *J. Vis. Exp.* **2015**, *2015*, 53051. [CrossRef] [PubMed]
126. Streets, A.M.; Huang, Y. Chip in a Lab: Microfluidics for next Generation Life Science Research. *Biomicrofluidics* **2013**, *7*, 1–23. [CrossRef] [PubMed]
127. Damiati, S.; Kompella, U.B.; Damiati, S.A.; Kodzius, R. Microfluidic Devices for Drug Delivery Systems and Drug Screening. *Genes* **2018**, *9*, 103. [CrossRef] [PubMed]
128. Zhu, Y.; Fang, Q. Analytical Detection Techniques for Droplet Microfluidics-A Review. *Anal. Chim. Acta* **2013**, *787*, 24–35. [CrossRef]
129. Tsui, J.H.; Lee, W.; Pun, S.H.; Kim, J.; Kim, D.H. Microfluidics-Assisted in Vitro Drug Screening and Carrier Production. *Adv. Drug Deliv. Rev.* **2013**, *65*, 1575–1588. [CrossRef]

130. Thomas, A.; Tan, J.; Liu, Y. Characterization of Nanoparticle Delivery in Microcirculation Using a Microfluidic Device. *Microvasc. Res.* **2014**, *94*, 17–27. [CrossRef]
131. Tammaro, O.; Costagliola di Polidoro, A.; Romano, E.; Netti, P.A.; Torino, E. A Microfluidic Platform to Design Multimodal PEG—Crosslinked Hyaluronic Acid Nanoparticles (PEG-CHANPs) for Diagnostic Applications. *Sci. Rep.* **2020**, *10*, 6028. [CrossRef]
132. Ahn, J.; Ko, J.; Lee, S.; Yu, J.; Kim, Y.; Li Jeon, N.; Woodruff, G.W. Microfluidics in Nanoparticle Drug Delivery; From Synthesis to Pre-Clinical Screening. *Adv. Drug Deliv. Rev.* **2018**, *128*, 29–53. [CrossRef]
133. Jurinjak Tušek, A.; Šalić, A.; Valinger, D.; Jurina, T.; Benković, M.; Kljusurić, J.G.; Zelić, B. The Power of Microsystem Technology in the Food Industry—Going Small Makes It Better. *Innov. Food Sci. Emerg. Technol.* **2021**, *68*, 102613. [CrossRef]
134. Miličević, N.; Panić, M.; Valinger, D.; Cvjetko Bubalo, M.; Benković, M.; Jurina, T.; Gajdoš Kljusurić, J.; Radojčić Redovniković, I.; Jurinjak Tušek, A. Development of Continuously Operated Aqueous Two-Phase Microextraction Process Using Natural Deep Eutectic Solvents. *Sep. Purif. Technol.* **2020**, *244*, 116746. [CrossRef]
135. Bačić, M.; Ljubić, A.; Gojun, M.; Šalić, A.; Tušek, A.J.; Zelić, B. Continuous Integrated Process of Biodiesel Production and Purification—The End of the Conventional Two-Stage Batch Process? *Energies* **2021**, *14*, 403. [CrossRef]
136. James, M.; Revia, R.A.; Stephen, Z.; Zhang, M. Microfluidic Synthesis of Iron Oxide Nanoparticles. *Nanomaterials* **2020**, *10*, 2113. [CrossRef]
137. Bennett, J.A.; Campbell, Z.S.; Abolhasani, M. Role of Continuous Flow Processes in Green Manufacturing of Pharmaceuticals and Specialty Chemicals. *Curr. Opin. Chem. Eng.* **2019**, *26*, 9–19. [CrossRef]
138. Wang, X.; Liu, J.; Wang, P.; deMello, A.; Feng, L.; Zhu, X.; Wen, W.; Kodzius, R.; Gong, X. Synthesis of Biomaterials Utilizing Microfluidic Technology. *Genes* **2018**, *9*, 283. [CrossRef]
139. Ma, J.; Wang, Y.; Liu, J. Biomaterials Meet Microfluidics: From Synthesis Technologies to Biological Applications. *Micromachines* **2017**, *8*, 255. [CrossRef]
140. Niculescu, A.G.; Chircov, C.; Bîrcă, A.C.; Grumezescu, A.M. Nanomaterials Synthesis through Microfluidic Methods: An Updated Overview. *Nanomaterials* **2021**, *11*, 864. [CrossRef]
141. Abiev, R.S.; Almjasheva, O.V.; Popkov, V.I.; Proskurina, O.V. Microreactor Synthesis of Nanosized Particles: The Role of Micromixing, Aggregation, and Separation Processes in Heterogeneous Nucleation. *Chem. Eng. Res. Des.* **2022**, *178*, 73–94. [CrossRef]
142. Yao, C.; Liu, Y.; Zhao, S.; Dong, Z.; Chen, G. Bubble/Droplet Formation and Mass Transfer during Gas–Liquid–Liquid Segmented Flow with Soluble Gas in a Microchannel. *AIChE J.* **2017**, *63*, 1727–1739. [CrossRef]
143. Yao, C.; Liu, Y.; Xu, C.; Zhao, S.; Chen, G. Formation of Liquid–Liquid Slug Flow in a Microfluidic T-Junction: Effects of Fluid Properties and Leakage Flow. *AIChE J.* **2018**, *64*, 346–357. [CrossRef]
144. Dang, M.; Yue, J.; Chen, G.; Yuan, Q. Formation Characteristics of Taylor Bubbles in a Microchannel with a Converging Shape Mixing Junction. *Chem. Eng. J.* **2013**, *223*, 99–109. [CrossRef]
145. Zong, J.; Yue, J. Gas–Liquid Slug Flow Studies in Microreactors: Effect of Nanoparticle Addition on Flow Pattern and Pressure Drop. *Front. Chem. Eng.* **2022**, *3*, 788241. [CrossRef]
146. Tušek, A.J.; Anić, I.; Kurtanjek, Ž.; Zelić, B. Mass Transfer Coefficient of Slug Flow for Organic Solvent-Aqueous System in a Microreactor. *Korean J. Chem. Eng.* **2015**, *32*, 1037–1045. [CrossRef]
147. Etminan, A.; Muzychka, Y.S.; Pope, K. Liquid Film Thickness of Two-Phase Slug Flows in Capillary Microchannels: A Review Paper. *Can. J. Chem. Eng.* **2022**, *100*, 325–348. [CrossRef]
148. Wu, Z.; Cao, Z.; Sunden, B. Flow Patterns and Slug Scaling of Liquid-Liquid Flow in Square Microchannels. *Int. J. Multiph. Flow* **2019**, *112*, 27–39. [CrossRef]
149. Zhang, Q.; Liu, H.; Zhao, S.; Yao, C.; Chen, G. Hydrodynamics and Mass Transfer Characteristics of Liquid–Liquid Slug Flow in Microchannels: The Effects of Temperature, Fluid Properties and Channel Size. *Chem. Eng. J.* **2019**, *358*, 794–805. [CrossRef]
150. Hakke, V.; Sonawane, S.; Anandan, S.; Sonawane, S.; Ashokkumar, M. Process Intensification Approach Using Microreactors for Synthesizing Nanomaterials—A Critical Review. *Nanomaterials* **2021**, *11*, 98. [CrossRef]
151. Suryawanshi, P.L.; Sonawane, S.H.; Bhanvase, B.A.; Ashokkumar, M.; Pimplapure, M.S.; Gogate, P.R. Synthesis of Iron Oxide Nanoparticles in a Continuous Flow Spiral Microreactor and Corning® Advanced Flow™ Reactor. *Green Process. Synth.* **2018**, *7*, 1–11. [CrossRef]
152. Göpfert, L.; Schoenen, M.; Reisen, O.; Buhl, E.M.; Mues, B.; Schmitz-Rode, T.; Slabu, I. Enabling Continuous Flow Manufacturing of Magnetic Nanoparticles with a Millifluidic System. *J. Magn. Magn. Mater.* **2022**, *563*, 169985. [CrossRef]
153. Ahrberg, C.D.; Choi, J.W.; Chung, B.G. Droplet-Based Synthesis of Homogeneous Magnetic Iron Oxide Nanoparticles. *Beilstein J. Nanotechnol* **2018**, *9*, 2413–2420. [CrossRef]
154. Panariello, L.; Wu, G.; Besenhard, M.O.; Loizou, K.; Storozhuk, L.; Thanh, N.T.K.; Gavriilidis, A. A Modular Millifluidic Platform for the Synthesis of Iron Oxide Nanoparticles with Control over Dissolved Gas and Flow Configuration. *Materials* **2020**, *13*, 1019. [CrossRef] [PubMed]
155. Larrea, A.; Sebastian, V.; Ibarra, A.; Arruebo, M.; Santamaria, J. Gas Slug Microfluidics: A Unique Tool for Ultrafast, Highly Controlled Growth of Iron Oxide Nanostructures. *Chem. Mater.* **2015**, *27*, 4254–4260. [CrossRef] [PubMed]
156. Aşık, M.D.; Kaplan, M.; Çetin, B.; Sağlam, N. Synthesis of Iron Oxide Core Chitosan Nanoparticles in a 3D Printed Microfluidic Device. *J. Nanopart. Res.* **2021**, *23*, 62. [CrossRef]

157. Abou Hassan, A.; Sandre, O.; Cabuil, V.; Tabeling, P. Synthesis of Iron Oxide Nanoparticles in a Microfluidic Device: Preliminary Results in a Coaxial Flow Millichannel. *Chem. Commun.* **2008**, *178*, 1783–1785. [CrossRef] [PubMed]
158. Uson, L.; Arruebo, M.; Sebastian, V.; Santamaria, J. Single Phase Microreactor for the Continuous, High-Temperature Synthesis of <4 nm Superparamagnetic Iron Oxide Nanoparticles. *Chem. Eng. J.* **2018**, *340*, 66–72. [CrossRef]
159. Anastas, P.T.; Warner, J.C. *Green Chemistry: Theory and Practice*; Oxford University Press: New York, NY, USA, 1998.
160. Ma, H.; Jin, N.; Zhang, P.; Zhou, Y.; Zhao, Y.; Zhang, X.; Lü, H.; Liu, J. Dynamic Characterization of Nanoparticles Production in a Droplet-Based Continuous Flow Microreactor. *Chem. Eng. Res. Des.* **2019**, *144*, 247–257. [CrossRef]
161. García-Merino, B.; Bringas, E.; Ortiz, I. Synthesis and Applications of Surface-Modified Magnetic Nanoparticles: Progress and Future Prospects. *Rev. Chem. Eng.* **2022**, *38*, 821–842. [CrossRef]